This is a preprint, the final version is subject to change, of the American Mineralogist (MSA)
Cite as Authors (Year) Title. American Mineralogist, in press.
(DOI will not work until issue is live.) DOI: http://dx.doi.org/10.2138/am-2016-5506

Revision 1

Amphibole thermometers and barometers for igneous systems, and some implications for eruption mechanisms of felsic magmas at arc volcanoes

Keith Putirka

Department of Earth and Environmental Sciences, California State University - Fresno, 2345 E. San Ramon Ave, MS/MH24, Fresno, CA 93720, kputirka@csufresno.edu

ABSTRACT

Calcic, igneous amphiboles are of special interest as their compositional diversity and common occurrence provide ample potential to investigate magmatic processes. But not all amphibole-based barometers lead to geologically useful information: recent and new tests reaffirm prior studies (e.g., Erdman et al. 2014), indicating that amphibole barometers are generally unable to distinguish between experiments conducted at 1 and and at higher pressures, except under highly restrictive conditions. And the fault might not lie with experimental failure. Instead, the problem may relate to an intrinsic sensitivity of amphiboles to temperature (T) and liquid composition, rather than pressure. The exceptional conditions are those identified by Anderson and Smith (1995): current amphibole barometers are more likely to be useful when T<800°C and $Fe\#^{amph} = Fe^{amph}/(Fe^{amph} + Mg^{amph}) < 0.65$. Experimentally grown and natural calcic amphiboles are here used to investigate amphibole solid solution behavior, and to calibrate new

thermometers and tentative amphibole barometers, that should be applicable to igneous systems generally.

Such analysis reveals that amphiboles are vastly less complex than may be inferred from published catalogs of end-member components. Most amphiboles, for example, consist largely of just three components: Pargasite ($NaCa_2(Fm_4Al)Si_6Al_2O_{22}(OH)_2$), Kaersutite ($NaCa_2(Fm_4Ti)Si_6Al_2O_{23}(OH)$) and Tremolite + Ferro-actinolite ($Ca_2Fm_5Si_8O_{22}(OH)_2$, where Fm = Fe + Mn + Mg). And nearly all remaining compositional variation can be described with just four others: Alumino-tschermakite ($Ca_2(Fm_3Al_2)Si_6Al_2O_{22}(OH)_2$), a Na-K-gedrite-like component ($(Na,K)Fm_6AlSi_6Al_2O_{22}(OH)_2$), a ferri-ferrotschermakite-like component ($Ca_2(Fm_3Fe^{3+}_2)Si_6Al_2O_{22}(OH)_2$), and an as yet unrecognized component with 3 to 4 Al atoms per formula unit (apfu), 1 apfu each of Na and Ca, and <6 Si apfu, here termed Aluminous Kaersutite: $NaCaFm_4Ti(Fe^{3+}, Al)Si_5Al_3O_{23}(OH)$. None of these components, however, are significantly pressure (*P*) sensitive, leaving the Al-in-amphibole approach, with all its challenges, the best existing hope for an amphibole barometer. A new empirical barometer based on D_{Al} successfully differentiates experimental amphiboles crystallized at 1 to 8 kbar, at least when multiple *P* estimates, from multiple amphibole compositions, are averaged. Without such averaging however, amphibole barometry is a less certain proposition, providing ± 2 kbar precision on individual estimates for calibration data, and ±4 kbar at best for test data; independent checks on *P* are thus needed. Amphibole compositions, however, provide for very effective thermometers, here based on D_{Ti}, D_{Na}, and amphibole compositions alone, with precisions of ±30ºC. These new models, and tests for equilibrium, are collectively applied to Augustine

volcano and the 2010 eruption at Merapi. Both localities reveal a significant cooling and crystallization interval (>190-270ºC) at pressures of 0.75 to 2.2 kbar at Augustine and Merapi respectively, perhaps the likely depths from which pre-eruption magmas are stored. Such considerable intervals of cooling at shallow depths indicate that mafic magma recharge is not a proximal cause of eruption. Rather, eruption triggering is perhaps best explained by the classic 'second boiling' concept, where post-recharge cooling and crystallization drive a magmatic system towards vapor saturation and positive buoyancy.

INTRODUCTION

Compared to other common silicate minerals, calcic, igneous amphiboles contain remarkable compositional diversity, and because of such, they may be un-equaled as records of magma compositions (e.g., Erdman et al. 2014), and magmatic pressures (*P*) and temperatures (*T*). However, while amphibole barometry has received considerable attention since the pioneering work of Hammerstrom and Zen (1986), tests by Erdman et al. (2014) show that existing amphibole geobarometers are not generally applicable to igneous systems. As will be shown, the earliest calibrations of Al-in-hornblende barometers (Hollister et al. 1987; Anderson and Smith 1995) are indeed still useful for near-solidus granitoids, under restricted conditions, but current barometers fare poorly when applied outside the conditions recommended by Anderson and Smith (1995), i.e., T<800ºC and $Fe\#^{amph} = Fe^{amph}/(Fe^{amph} + Mg^{amph}) < 0.65$.

A key problem is that amphibole barometry may be limited by its inherent inexactitude. As noted by Anderson and Smith (1995), we still do not understand the

equilibria that control Al partitioning into amphibole. And, of course, models based on highly restrictive conditions or compositions, necessarily exclude most igneous systems from analysis. Experimental and natural amphibole compositions are thus re-examined to better understand solid solution behavior and to calibrate new, empirical thermometers, which are generally applicable to igneous systems, and some tentative barometers which may be useful when combined with independent estimates of pressure.

BACKGROUND

The Al-in-hornblende barometer of Hammerstrom and Zen (1986) is one of the most influential petrologic tools yet calibrated—and for good reason. Their barometer was immediately used to place granitic magmatism within a crustal framework (e.g., Ague and Brimhall, 1988; Pickett and Saleeby 1993), and led to a number of new calibrations (e.g., Hollister et al. 1987; Johnson and Rutherford 1989; Schmidt 1992; Anderson and Smith 1995). More recently Ridolfi and Renzulli (2011) have calibrated a hornblende-only barometer, and other models for volcanic systems, and Molina et al. (2015) have a new amphibole thermometer and saturation model. But in this recent cases the data used for testing and calibration are limited: n = 20 to 61 for Ridolfi and Renzulli (2011) and n = 148 for Molina et al. (2015), compared to the >550 experimental data currently available. Ridolfi and Renzulli (2011) recognize that experimental error can limit model precision, and they show that amphibole compositions alone can be used to predict magmatic intensive variables. Here we explore the usefulness of such models using a much larger data set.

Because of the *T*-sensitivity of Al-in-hornblende and the potential for re-equilibration,

Blundy and Holland (1990) warned that without better thermal information, "the Al geobarometer is unlikely to be of much practical value"—a caveat that may be gleaned from Hammerstrom and Zen's (1987) Figs. 7 and 8. Anderson and Smith (1995) responded with a *T*-sensitive barometer. But as they make clear, useful *P* estimates derive only from highly restricted circumstances, e.g., near-solidus, multiply saturated granitic systems (see Hammerstrom and Zen 1986; Hollister et al. 1987), where $T < 800^{o}C$, and amphibole Fe/(Fe+Mg) <0.65 (Anderson and Smith 1995), and where multiple saturated phases and contact metamorphic rocks allow for independent estimates of *P* (e.g. Hollister et al. 1987; Anderson 1996; Anderson et al. 2008; Barnes et al. 2012).

Amphibole-based barometry is in fact fraught with very real and under-appreciated challenges. To illustrate, newer experimental data (Fig. 1) are used to reproduce Hammerstrom and Zen's (1987) Figs. 7B and 8, showing respectively the variation of total Al (Al^T, calculated on the basis of 23 oxygens) with *P* and *T*. The addition of ~500 experimental observations since 1987 change Al^T-*P* patterns very little: 1 kbar experiments yield amphiboles with a range of Al^T that encompasses more than half of all Al^T observed at any pressure, and Al^T at *P*=5 kbar that encompasses most observations at 20 kbar, and all four of the 25 kbar data. Note also that the maximum Al^T (>3.1in Fig. 1, all from Koester et al. 2002) occurs at 15 kbar, and these data exhibit nearly 20% internal variation that depends almost solely on *T* (Fig. 1b). Aluminum contents of amphiboles are clearly more sensitive to *T* (Fig. 1b) and Al_2O_3 contents of co-existing liquids (Fig. 1c) than to *P* (Fig. 1a, d, e). The *T*-sensitivity is especially evident when Al^T is compared to Si in amphibole, for which it mostly substitutes: except for a few high-Al^T outliers, amphiboles crystallized in the *P* range of 0-2 kbar encompass the entire span of Al^T-Si at

6-10 kbar (Fig. 2a). In contrast, when separated into *T* intervals, mean Si and Al^T contents systematically decrease and increase respectively, from 650 to 1175 ºC (Fig. 2b).

The challenges facing amphibole barometry can be further illustrated from a thermodynamic point of view. If a *P*-signal can be extracted, such should be driven by molar volume contrasts between competing amphibole components and co-existing liquids. We have the jadeite-in-pyroxene barometer (Putirka et al. 1996, 2003) as a useful benchmark. To evaluate the potential of amphibole barometry, thermodynamic data from Holland and Powell (1998) and the models of Lange and Carmichael (1990) (Table 1) are used for molar volume calculations (Table 1), where amphibole-melt equilibria are compared to the jadeite-in-pyroxene system. Table 1 reveals that amphibole-related molar volume contrasts are comparatively small. For example, the Al-rich pargasite ($NaCa_2(Mg_4Al)Si_6Al_2O_{22}(OH)_2$) component has a molar volume only ~0.3% less than tremolite ($Ca_2(Mg_5)Si_8O_{22}(OH)_2$), while jadeite ($NaAlSi_2O_6$) is 8% less than that for diopside ($CaMgSi_2O_6$). More importantly, liquid components that precipitate jadeite decrease their collective molar volume by nearly 38%—more than double the decrease by precipitation of diopside (17.8%). This larger reduction in volume for the jadeite-liquid equilibrium (compared to Di-liq) provides an incentive for pyroxene-saturated magmas to crystallize increasingly jadeite-rich pyroxenes at higher pressures. For amphiboles, by contrast, molar volume differences upon crystallization are much smaller and less well differentiated (Table 1). From such comparisons we might anticipate that pyroxene-based barometers should be nearly 7 times more sensitive to *P* than their amphibole counterparts; and even the pyroxene-based barometers have standard errors of estimate

(or SEE; or model root mean square errors) that are not small: ±0.7 kbar when multiple estimates are averaged, ± 1.2-2.0 kbar for individual estimates (Putirka 2008).

These results do not impugn careful barometric results on near-solidus granitic systems, where *P* estimates are tested against independent igneous and metamorphic equilibria (e.g., Hollister et al. 1987; Anderson and Smith 1995; Anderson 1996; Anderson et al. 2008). However, it remains quite unclear that *P* can be predicted from amphibole in systems exhibiting high thermodynamic variance—igneous systems saturated with just one or a few phases. But while the prospects for amphibole barometry are dim, they are not utterly dark.

Experimental data provide a hint that a *P* signal might yet be extracted from amphiboles under more general circumstances. Formal amphibole-liquid equilibria (Fig. 1e) show no apparent variation with *P*/*T* (Fig. 1d, e), but the partition coefficient for Al, $D_{Al} = {Al^{amph}}/{X_{Al2O3}^{liq}}$ (where $Al^{amph} = Al^{T}$) increases with *P*/*T* systematically (Fig. 1d), albeit at a very low slope. Ridolfi and Renzulli (2011) argued that a stronger *P* signal could further be recovered by limiting calibrations to experiments that report small compositional errors, and that yield amphibole compositions most similar to those found in nature. There is merit in both arguments. Phase homogeneity should be a criterion for equilibrium, and Figures 3a and 3b show that experimental amphiboles vary widely with respect to Mg#, Si and Al^{T}. However, the Ridolfi and Renzulli (2011) data restrictions mean that <12% of current experimental data are used. This may reject possibly useful data, where compositional errors are not reported; there is value in performing calibrations on data that span a wider range of compositions compared to nature, to minimize or eliminate model extrapolation. We might also reject data where crystals

approximate equilibration despite exhibiting heterogeneity; all crystals are heterogeneous; what critical value of heterogeneity do we reject? In any case, errors on the Ridolfi and Renzulli (2011) barometers are not correlated with compositional error, which calls into question the application of a heterogeneity filter.

METHODS

Natural amphibole compositions (n = 1,165) are from Ridolfi and Renzulli (2011). Experimental data (n = 560) are from LEPR (Hirschmann et al., 2008) and other published experiments where liquid compositions are reported to be saturated with amphibole (Fig. 1). Ninety-five percent (n = 531) of experimental amphiboles are 'calcic' (Leake et a. 1997), falling into the magnesiohornblende, tschermakite and ferrortchermakite fields; of the remainder, 4 samples are 'sodic-calcic' and the rest (n=25) are in the Mg-Fe-Mn-Li group (Leake et al. 1997). The sodic-calcic amphiboles mostly fall well outside compositional trends formed by the remaining amphiboles and so are not used for test or calibration purposes. Several Mg-Fe-Mn-Li amphiboles are similarly aberrant, but Mg-Fe-Mn-Li amphiboles from DiCarlo et al. (2010) and Scaillet and MacDonald (2003), at T=661-731ºC, fall on the same Si^{amph} v. Al^{amph} trends as calcic amphiboles, with Si^{amph} >7.8 and Al^{amph} <0.5 atoms per 23 oxygens; these are retained as test data. All amphiboles used for calibration are calcic, and the term "amphibole" herein implies mostly calcic compositions.

The models are mostly derived by step-wise linear least square regression, using a thermodynamic formalism for the regression equations (see Putirka 2008); non-linear regression methods are used for some thermometers, guided by linear least-squares

results. For linear least squares models, leverage plots are used to assess whether a given variable is useful. More importantly, a trial-and-error approach is applied to decide which data to include for calibration, and which variables to included in any model. The foremost goal of such trials is to find a small subset of data to use for calibration Data Set 1 or DS1) that can successfully predict a dependent variable from all other data, designated as test data or DS2, i.e., data not used for calibration. For calibration, 156 data are used (Data Set 1 or DS1), which feature internally consistent and coherent *T* - composition trends. For some regressions, one or a few data points from DS1 fall off coherent trends, and such data are not used for calibration. Most all data rejected for calibration are put into DS2, but data that fall far from coherent *T*-composition trends are rejected entirely. Data set 3 (DS3) is a subset of all data from DS1 and DS2 where T<800ºC and $Fe\#^{amph}$<0.65.

Most experimental liquids are multiply saturated, but variably so, and few contain the complete list of phases (e.g., quartz + plagioclase + alkali feldspar + biotite + Fe-Ti oxides + titanite + fluid) often recommended for Al-in-hornblende barometry (e.g., Anderson 1996). These data thus disallow rigorous tests of models such as Hollister et al. (1987) and Anderson and Smith (1995). But we can make use of a much broader spectrum of data to discover whether *P* and *T* can be reliably predicted not just for near-solidus granitoids, or a small subset of experimental data, but for a wide range of igneous systems.

Experimental data are divided into calibration (n≈158) and test data sets (n≈383), with the goal of using as few data as possible for calibration, and as many as possible for test purposes. Calibration data are selected somewhat intuitively, based on coherence in

regression analysis, and the ability of individual data to describe variations in *P, T* and composition (see Putirka 2008), but besides using calcic amphiboles, no compositional restrictions or restrictions on *P*, *T* or phase appearance (besides amphibole and liquid) are applied.

Liquid and amphibole components are calculated in two ways. To investigate amphibole solid solution behavior we use exchange components, as in Thompson (1982). Trial an error leads to two natural formulas, cummingtonite and tremolite, and a third fictive stoichiometric component $Si_{11.5}O_{22}(OH)_2$, that can be combined with five exchange components (Table 2); these describe nearly all amphiboles as a set of positive components. The fictive component, $Si_{11.5}O_{22}(OH)_2$ approaches zero for most natural amphibole compositions (although it may be significantly positive for low-Al, high-Si compositions). Natural amphiboles can be converted to exchange components by multiplying a row matrix of amphibole cation fractions: SiO_2, TiO_2, $AlO_{1.5}$, FmO, CaO, $NaO_{0.5}$, $KO_{0.5}$ (where FmO = FeO + MnO + MgO) against the inverse matrix of Table 2, shown as Table 3. A worked out example is given in Table 4a. Although this procedure allows one to describe amphiboles as a sum of mostly positive components, its use here is to provide compositional extrema, which are used to decipher solid solution trajectories.

For the purposes of thermometry and barometry, we calculate components as follows: for amphiboles, cations are calculated on the basis of 23 oxygens (Table 4b), and like co-existing liquids, we take total Fe as FeOt. For the purposes of thermometry and barometry, Fe^{3+} is ignored, as spectroscopic work has demonstrated, as with pyroxenes, that Fe^{3+} calculated from stoichiometry (e.g., Leake et al. 1997) has no correlation to measured values (Hawthorne 1983; Dyar et al. 1992, 1993; Almeev et al. 2002). Whne

fO_2 is known, Fe^{3+} is calculated to investigate solid solution trajectories only, making use of King et al.'s (2000) observation that Fe^{3+}/Fe^{2+} ratios are the same in coexisting amphiboles and liquids. But fO_2 does not affect the partitioning of elements that are examined here for thermometry and barometry, i.e., Na, Ti and Al. Except for one barometer (not recommended) liquids are calculated as hydrous mole fractions, where all water is taken as H_2O, cations are as SiO_2, Al_2O_3, TiO_2, Na_2O, etc., and all Fe is taken as FeOt (for FeO total) (Table 4c). This approach means that one must estimate water in a given system before estimating *P* and *T*; but as will be shown, *T* estimates are affected very little by such assumptions (<2°C per 1 wt. % H_2O), and the most useful barometers (where *P* estimates increase at a rate of 0.4 kbar per 1 wt. % H_2O) are derived only by accounting for water, implicitly or explicitly. For experimental data, where water is not measured, it is estimated by taking the difference between 100 and the reported anhydrous oxide sum.

Sample calculations for liquid and amphibole components and *P-T* estimates, from this work and from a number of published studies, are provided in Tables 4a-c. A spreadsheet for performing all calculations is available as Electronic Supplement A.

RESULTS

Describing Experimentally-grown and Natural Amphibole Compositions

Natural amphiboles are notorious for their compositional complexity, and crystallographers, seeking the novel, have identified dozens of end-members (Leake et al. 1997). Stoichiometric analysis shows (Figs. 3 and 4), however, that most of the compositional variation of experimental and natural amphiboles can be described as solid

solutions of just three components: Tremolite + Ferro-actinolite ($Ca_2Fm_5Si_8O_{22}(OH)_2$, where Fm = Fe + Mn + Mg), Pargasite ($NaCa_2(Fm_4Al)Si_6Al_2O_{22}(OH)_2$) and Kaersutite ($NaCa_2(Fm_4Ti)Si_6Al_2O_{23}(OH)$). And just four other components are needed to describe all remaining compositions. An Alumino-tschermakite component ($Ca_2(Fm_3Al_2)Si_6Al_2O_{22}(OH)_2$) is useful for describing amphiboles with high Al at moderate Si; a Na-K-gedrite-like component (gedrite = $NaFm_6AlSi_6Al_2O_{22}(OH)_2$) describes high Na and high K (Fig. 4) varieties; and a ferri-ferrotschermakite-like component ($Ca_2(Fm_3Fe_3^{+2})Si_6Al_2O_{22}(OH)_2$; not shown) can explain Fe^{3+} variation. Perhaps most interesting is a final and rather significant component that is not evident in the myriad stoichiometries of Leake et al. (1997). Experimental and natural amphiboles often contain <6 Si atoms per formula unit (apfu) and trend toward a stoichiometry with one cation each of Na and Ca, 3 to 4 cations of Al, and 1 cation of Ti per formula unit; this fictive end-member is not quite canniloite or sadanagaite (see Leake et al. 1997) and may involve Fe^{3+}; it is here termed Aluminous Kaersutite (Al-K), with an approximate stoichiometry of $NaCaFm_4Ti(Fe^{3+}, Al)Si_5Al_3O_{23}(OH)$. This new component represents yet another lacuna in our understanding of amphibole chemistry, which hopefully may entice crystallographers away from the exotic, as tempting as such may be. This identification of actual solid solution components is important as it can sharpen our focus of the crystallographic and calorimetric data that are most needed to advance thermobarometric calibrations and models of silicate liquid crystallization (e.g., Ghiorso et al. 1995).

A Test for Equilibrium

While the amphibole exchange components introduced in Tables 2 and 3 provide a near complete description of natural magmatic amphiboles, none lead to equilibria that that are *P*-sensitive. But the empirical approach of Ridolfi and Renzulli (2011) provides a valuable avenue to calibrate remarkably precise thermometers, and perhaps even a useful barometer. First, though, we consider a test for amphibole-liquid equilibrium, following the approach of Roeder and Emslie (1970) for olivine. The Fe-Mg exchange coefficient $K_D(\text{Fe-Mg})^{\text{amph-liq}}$ (herein, simply K_D) is independent of *P* or *T* ($R^2 = 0.08$ and 0.1 respectively) and composition and is written as:

$$K_D = \frac{\frac{X_{FeOt}^{amph}}{X_{MgO}^{amph}}}{\frac{X_{FeOt}^{liq}}{X_{MgO}^{liq}}} \qquad (1)$$

where FeOt is total Fe as FeO. It is numerically equivalent to taking the numerator as Fe_t^{amph}/Mg^{amph}, where the indicated elements are amphibole cations on a 23 oxygen basis, and Fe_t is total Fe as Fe^{2+}. The 10th and 90th percentiles for K_D are 0.13 to 0.41 respectively (n = 457; values trending to >>0.5 are excluded). This broad range in K_D may attest to a resistance of amphibole to equilibrate in experimental systems, but may still be useful as a liberal test of equilibrium. A more restrictive test can be obtained from the mean and standard deviation:

$$K_D = 0.28 \pm 0.11 \qquad (2)$$

An important caveat is that equilibration of Fe-Mg exchange can be independent of Na or Al exchange, and so may not be a flawless guide to equilibrium for thermometry and barometry, based on D_{Al} and D_{Na} respectively. But it can be used to decipher whether an amphibole is at least a plausible candidate for having equilibrated from a given liquid.

Thermometers and Barometers

Of several recent thermometers, the liquid-only model of Molina et al. (2015) and Ridolfi and Renzulli's (2011) amphibole-only model are best, allowing prediction of *T* to within ±50ºC (Figs. 5a-c). But the chemography of Figure 4b may provide a guide towards more broadly applicable models. Clearly, Si in amphibole varies strongly with *T*, and provides a remarkably simple thermometer: *T*(ºC) = 1977 + 165[Si] (or [Si] = 10.9 – 0.0048T(ºC)), with SEE = ±44ºC (or ±0.23 apfu), and R^2 = 0.80 (n = 161). This is by no means a recommended model, but serves to illustrate that thermal variations alone can account for >75% of the variations in Si, at least in our calibration data set. Moreover, unlike other ferromagnesian silicates, Mg# in amphibole varies inversely with *T*, so in the typical Mg# v. Si classification plot (Leake et al. 1997), *T* generally increases in the direction of lower Si and higher Mg# (as well as higher Al, Na, and Ti).

As in Molina et al. (2015), it is possible to predict *T* from liquid compositions alone, and a rather precise *P*-independent amphibole "saturation surface" is:

$$T(^{o}C) = \frac{24429.2}{2.31+42.1\left[X_{FeOt}^{liq}\right]+32.2\left[X_{CaO}^{liq}\right]+2.21\left[\ln\left(X_{SiO_2}^{liq}\right)\right]-1.4\left[ln(X_{TiO_2}^{liq})\right]-2.666[\ln\left(X_{FmAl}^{liq}\right)]} \qquad (3)$$

Here, *T* represents the temperature at which amphibole should appear for a given liquid composition, and X_i are the hydrous mole fractions of oxides in an amphibole saturated liquid. Calibration data are from sources listed in the caption of Fig. 5. Error is ±33 ºC, with R^2 = 0.91 (n=154) (Fig. 5d). Pressure ranges from 0.5 to 25 kbar for the calibration data, but adding *P* as a variable does not significantly improve *T* prediction. Thermometers based on D_{Na}, and D_{Ti}, also *P*-independent, provide links to observed amphibole compositions and decreas error by about 17%:

$$T(^oC) = \frac{6383.4}{-12.07 + 45.4\left[X_{Al2O3}^{liq}\right] + 12.21\left[X_{FeOt}^{liq}\right] - 0.415\left[X_{TiO2}^{liq}\right] - 3.555\left[\ln\left(X_{Al2O3}^{liq}\right)\right] - 0.832\left[ln(X_{Na2O}^{liq})\right] - 0.481[\ln\left(X_{FeOt}^{liq}X_{Al2O3}^{liq}\right)] - 0.679[\ln\left(D_{Na}\right)]} \quad (4a)$$

$$T(^oC) = \frac{8037.85}{3.69 - 2.62\left[X_{H2O}^{liq}\right] + 0.66\left[Fe_{total}^{amph}\right] - 0.416\left[\ln\left(X_{TiO2}^{liq}\right)\right] + 0.37\left[\ln\left(X_{MgO}^{liq}\right)\right] - 1.05[\ln\left(X_{FeOt}^{liq}X_{Al2O3}^{liq}\right)] - 0.462[\ln\left(D_{Ti}\right)]} \quad (4b).$$

In Eqns. (4a) and (4b), X_i^{liq} are hydrous mole fractions of the indicated oxides. The terms D_{Na} (Eqn. 4a) and D_{Ti} (Eqn. 4b) are the partition coefficients of Na and Ti, taken as a ratio of the number of Na or Ti cations in amphibole on a 23 oxygen basis (Na^{amph} or Ti^{amph}), divided by the hydrous mole fraction of Na_2O or TiO_2 in co-existing liquid (X_{Na2O}^{liq}, or X_{TiO2}^{liq}): so we have $D_{Na} = {Na^{amph}}/{X_{Na2O}^{liq}}$. In Eqns. 4a, and 4b, X_i are the mole fractions of oxides in the superscripted phase. Although the use of hydrous mole fractions means that Eqns. 3-4 are implicitly sensitive to H_2O, the affect is small: T varies <2ºC per 1 wt. % change in H_2O. This is an artifact of the calculation scheme, but not inconsistent with experimental phase equilibria that indicate that amphibole saturation is mostly independent of H_2O (e.g., Moore and Carmichael 1998; Barclay and Carmichael 2004). Both thermometers are calibrated using data used to calibrate Eqn. (3), with the addition of data (the Mg-Fe-Mn-Li amphiboles) from DiCarlo et al. (2010), leaving the Mg-Fe-Mn-Li amphiboles from Scaillet and MacDonald (2003) as a test. Equation (4a) reproduces experimental temperatures to ±23 ºC, with $R^2 = 0.93$; n = 155, whereas Eqn. (4b) has SEE = ± 24ºC, $R^2 = 0.92$ and n = 153 (Figs. 5e, f). Equations 4a and 4b can be used to test for equilibrium, to the extent that both thermometers agree.

Interestingly, however, thermometers are no worse, and in some cases better, when relying on amphibole compositions alone, as in Ridolfi and Renzulli (2011). A *P*-independent thermometer is:

$$T(^{o}C) = 1781 - 132.74[Si^{amph}] + 116.6[Ti^{amph}] - 69.41[Fe_t^{amph}] + 101.62[Na^{amph}] \quad (5)$$

And if *P* is known,

$$T(^{o}C) = 1687 - 118.7[Si^{amph}] + 131.56[Ti^{amph}] - 71.41[Fe_t^{amph}] + 86.13[Na^{amph}] + 22.44[P(GPa)] \quad (6)$$

In these equations, terms such as Si^{amph}, Ti^{amph}, and Na^{amph}, are the numbers of the indicated cations in amphibole, when calculated on the basis of 23 oxygens; Fe_t^{amph} represents the total number of Fe cations, calculated as FeO. In the *P*-independent model (Eqn. 5), the calibration data are reproduced to ±30°C; adding *P* as an independent variable (Eqn. 6) reduces error to ±28°C (Figs. 5g, h).

Finally, three tentative amphibole-liquid barometers are calibrated as

$$P(kbar) = -30.93 - 42.74[ln(D_{Al})] - 42.16\left[ln\left(X_{Al2O3}^{liq}\right)\right] + 633\left[X_{P2O5}^{liq}\right] + 12.64\left[X_{H2O}^{liq}\right] + 24.57[Al^{amph}] + 18.6[K^{amph}] + 4.0[ln(D_{Na})] \quad (7a)$$

$$P(kbar) = -64.79 - 6.064[ln(D_{Al})] + 61.75\left[X_{SiO2}^{liq}\right] + 682\left[X_{P2O5}^{liq}\right] - 101.9\left[X_{CaO}^{liq}\right] + 7.85[Al^{amph}] - 46.46[\ln\left(X_{SiO2}^{liq}\right)] - 4.81\left[ln\left(X_{Na2O}^{liq} + X_{K2O}^{liq}\right)\right] \quad (7b)$$

$$P(kbar) = -45.5 - 46.3\left[ln\left(D_{Al}^{anhyd}\right)\right] - 41.1\left[ln\left(X_{Al2O3}^{anhyd}\right)\right] + 439\left[X_{P2O5}^{anhyd}\right] + 26.6[Al^{amph}] + 22.5[K^{amph}] + 5.23\left[ln\left(D_{Na}^{anhyd}\right)\right] \quad (7c)$$

Terms in Eqns. (7a) and (7b) are as in Eqns. (5-6), where all liquid composition terms are hydrous mole fractions of the indicated oxides, and the partition coefficient terms in (7a), and (7b), i.e., D_{Na} and D_{Al} (e.g., where $D_{Na} = {Na^{amph}}/{X_{Na2O}^{liq}}$ and $D_{Al} = {Al^{amph}}/{X_{Al2O3}^{liq}}$) use hydrous mole fractions for the liquid, In Eqn. (7c), terms such as X_{Al2O3}^{anhyd} are anhydrous mole fractions and D_{Na}^{anhyd} and D_{Na}^{anhyd} denote the use of anhydrous liquid components in the denominator of the partition coefficients. The partition coefficients are merely fit parameters, whose key attribute is that they help differentiate between 2 and 8 kbar systems. Note, for example, that in each of Eqns. (7a-c) that the coefficient on $\ln D_{Al}$ is negative. Equation (7a) is preferred, being more precise (Fig. 6d), but 7b may be more precise at low T (Fig. 6e), and exhibits less systematic error at >10 kbar (Fig. 7c). Both Eqns. (7a), and (7b) are sensitive to estimated water contents (the liquid components in 7b vary with water contents), with P estimates that increase at a rate of ~0.4 kbar per 1 wt. % increase in H_2O. Equation (7c) is an anhydrous version of (7a); it is not recommended except as a crude check, as it is less precise (Fig. 6f), but it illustrates the utility of including water contents for P estimation, either explicitly (Eqn. 7a) or implicitly (Eqn. 7b). The X_{P2O5}^{liq} terms in Eqns. (7a-c) may come as a surprise, but t-ratios are ≈6, and the terms allow more accurate prediction of pressures for data not used for calibration, when P_2O_5 is known. Calibration data are as for Eqn. 3, with the addition of Koester et al. (2002). Equations (7a) and (7c) do not apply to Mg-Fe-Mn-Li amphiboles, which were precipitated at 1.5 kbar (these models predict pressures of 40-50 kbar) as might be gathered from the anomalously low D_{Al} values at a given P/T (Fig. 1d, f); Eqn. (7b) comes close within error of 1.5 kbar, with predicted pressures of ~1 atm, but the barometers should probably only be applied to calcic amphiboles. For Eqns. (7a), and

(7b), $R^2 = 0.9$, and SEE = ±1.6 and ±1.7 kbar respectively (n = 156) for the calibration data. All equations are tested using "test data", i.e., data not used for calibration (Figs. 5, 6; Data Set 2 or DS2). Calibration data are noted as Data Set 1 (DS1).

As noted, almost none of the experimental data collected for this study are saturated in the 7-10 crystalline phases often recommended for Al-in-hornblende barometry (e.g., Anderson 1996), which would seem to limit our ability to test such models. But Anderson and Smith (1995) recommend two filters, which are readily applied: T<800°C and $Fe\#^{amph} = Fe^{amph}/(Fe^{amph} + Mg^{amph}) < 0.65$. These conditions remove 90% of the ~541 data used for test and calibration purposes. But the Anderson and Smith (1995) conditions are less arbitrary: they do not imply, for example, that some experiments are "good" while others are "bad". Under their restrictions, most models are indeed able to differentiate between 1 atm and 8 kbar pressures (Figs. 6g-j), with errors that likely approach the limits of condensed phase barometry. These results appear to validate the Anderson and Smith (1995) approach, and also call into question the extent to which multiple saturation is a relevant test of model applicability.

DISCUSSION

Amphibole Compositions

By applying the approach of Thompson (1982) it is possible to uncover stoichiometric substitutions that control amphibole solid solution. Such analysis shows that both experimental and natural amphibole systems not only are compositionally quite similar, but also vary by the same stoichiometric substitutional mechanisms. Thus, while experimentally grown amphiboles exhibit wide variation, they exhibit the same solid

solution behaviors exhibited in nature. This analysis further shows that natural amphiboles are vastly more simple than might be ascertained by the numerous end-member components so far identified (e.g., Leake et al., 1997). However, at least one important natural amphibole component, with 3 to 4 Al apfu, 1 apfu each of Ca and Na apfu, and <6 Si apfu has yet to be described by crystallographers; this belies the suggestion by Hawthorne (2012) that further ambient crystallographic work on rock-forming minerals cannot be justified. Components derived from such analysis can prove useful as thermometers. Our Eqn. (4b) for example, is effectively a kaersutite-liquid thermometer (in a normative scheme, kaersutite would be defined as the lesser of Ti or Na on the basis of 23 oxygens). But no formal equilibrium expression examined here provides a barometer as precise as when using D_{Al}, which validates the empirical approach of Hammerstrom and Zen (187) and Ridolfi and Renzulli (2011), etc., with their emphasis on Al^{T}.

Thermobarometry and Hygrometry—Challenges and Recommended Approaches

The current challenge to amphibole barometry is that unless highly restrictive conditions are applied (e.g., Anderson and Smith 1995; Ridolfi and Renzulli 2011) amphibole barometers are unable distinguish 1 kbar from 5 kbar or 8 kbar experiments (Figs. 1, 2; also see Erdman et al. 2014)—a pressure range of particular interest for crustal evolution and felsic magmatism. Even using the best of Ridlofi and Rnzulli's (2011) equations (their model 1d), or the new models calibrated here (Eqns. 7a, b), *P* estimates on individual experiments in our test data set are no better than ~±4 kbar. And there is no highly precise test for an approach to equilibrium. For example, if we predict

P only for those test data (DS2) where K_D = 0.27-0.33, the SEE drops from ±3.6 to ±3.0 kbar (and R^2 = 0.61; n = 115), a significant decrease, but still at the ragged edge of usefulness. With such error, *P* estimates on individual natural amphibole grains do little more than place crystallization somewhere above the Moho.

It is also unclear that the addition of co-existing phases solves the problem. Hammerstrom and Zen (1986) suggest that because Al and Si are highly correlated (see Figs. 2-3), Al-in-hornblende barometry might be more precise for quartz-saturated liquids, since this should limit Si in amphibole, leaving *P* to control variation in Al. But *P* is not better predicted in quartz saturated or otherwise high SiO_2 systems. Aluminum contents in amphibole are, generally, not strongly sensitive to *P*, and no model of activity can compensate for a low ΔV_r.

In light of these caveats, new barometers, based on D_{Al} (Eqns. 7a,b), and making use of H_2O as input (Eqns. 7a, 7b), allow us to distinguish *P* estimates in the 1 kbar to 8 kbar range, to ±1 kbar (Fig. 7a), when multiple estimates are averaged. But accurate P estimates in nature will require independent tests of *P* and *T*. It is thus recommended that Equations 7a and 7b are compared to one another, and perhaps also to Ridolfi and Renzulli (2012) model 1d, preferring the latter, or 7b, at *P*>10 kbar. Amphibole *P-T* results should also be compared to (a) clinopyroxene-derived pressures if possible (e.g., Putirka et al. 2003) or (b) *T* estimates from other silicates, with comparisons to experimental phase relationships (e.g., Moore and Carmichael 1998; Barclay and Carmichael 2004; Holtz et al. 2005) for consistency.

As to hygrometry, the same experimental data that allow us to calibrate remarkably precise thermometers (DS1) fail to yield a model that, from amphibole components alone,

can predict H_2O contents of co-existing liquids. Such models describe little more than ~25% of total H_2O variations for test data (DS2). This perhaps relates to the insensitivity of amphibole saturation to *T* (e.g., Moore and Carmichael 1998; Blatter and Carmichael 2001), or complex effects of water on amphibole saturation (Ghiorso 1999; Maksimov 2009). But there are also numerical issues: most experiments are conducted at water-saturated conditions, and so have limited and overlapping water contents, which limit regression leverage. For example, where water is directly measured and $P \leq 8$ kbar, mean water contents are 5.8±1.8% H_2O for the calibration data (n=99). At $P \leq 5$ kbar (n=148), 90% of experimental liquids have 3.6 to 8.3% H_2O, and half are in the range 5.4 to 6.9% H_2O (mean = 6.2±1.9%). These results help to delimit water contents when amphibole and vapor are co-saturated. And as might be expected, water contents are higher at greater pressure: at $P \leq 8$ kbar (n=178), mean H_2O contents are 6.4±2.6% (90% fall between 3.8 and 9.9 wt. % H_2O; half are between 5.5 and 7.8% H_2O). At 8 kbar < $P \leq 16$ kbar, the mean is 9.5±3.3% (n=74; 90% fall between 4.9 and 14.0 % and half are between 6.8 and 12.2%). But these modest changes do not appear to greatly control amphibole compositions. This does not preclude the possibility that fH_2, or perhaps fH_2O, might be derived from carefully measured Fe^{3+}/Fe^{2+} ratios and $(OH)^-$ concentrations in natural amphiboles (e.g., Popp et al. 1995). But the work of Ghiroso (1999) and Maksimov (2009) show a need for new amphibole saturation experiments at water undersaturated conditions, which may better address the true potential of amphibole hygrometry.

But with all the noise in our attempts to predict *P* and H_2O, we might ask: do the global experimental data provide a coherent view of amphibole-liquid equilibrium? The answer is that they do indeed yield thermometers with accuracies comparable to other

silicate-liquid systems (Putirka 2008; i.e., ±30 ºC). For example, using both DS1 + DS2, and amphibole components only we have:

$$T(^oC) = 1201.4 - 97.93[Si^{amph}] + 201.82[Ti^{amph}] + 72.85[Mg^{amph}] + 88.9[Na^{amph}] + 40.65[P(GPa)] \quad (8).$$

Or using a Na-K exchange coefficient (e.g., Helz 1979):

$$T(^oC) = \frac{10073.55}{9.75 + 0.934[Si^{amph}] - 1.454[Ti^{amph}] - 0.882[Mg^{amph}] - 1.123[Na^{amph}] - 0.322[\ln(X_{FeOt}^{liq})] - 0.15[\ln(K_D^{Na-K})] - 0.759[\ln(D_{Al})]} \quad (9).$$

The terms in Eqns. (8) and (9) are as in Eqns. (4-7); in Eqn. (9), $K_D^{Na\text{-}K}$ is the Na-K exchange coefficient of Helz (1979), $K_D^{Na\text{-}K} = (K^{amph}/Na^{amph})/(X_{K2O}^{liq}/X_{Na2O}^{liq})$, except here, Na^{amph} and K^{amph} are total Na and K cations on a 23 oxygen basis (instead of Helz's use of Na on the A site); X_{Na2O}^{liq} and X_{K2O}^{liq} are the hydrous mole fractions of the indicated oxides. Although Helz (1979) uses only Na on the A site, her expression for Na on the B site, $Na_B = 2 - Ca - Fe_{total}$, leaves almost no Na on the B site for most amphiboles, so our $K_D^{Na\text{-}K}$ is in most cases numerically identical to that of Helz (1979). Equation (8) recovers *T* on DS1+DS2 to ±47ºC (n = 539; Mg-Fe-Mn-Li amphiboles are excluded), while Equation (9) reduces error further, to ±39ºC (n=549) (Fig. 8), with just a ±27ºC uncertainty on DS1. While the global regressions preclude more rigorous testing, they show that *T*-compositions relationships are quite coherent and consistent. And Eqn. (9), being as precise as any model regressed on much smaller data sets, can be used to test the thermometers presented above, when applied to natural systems. Of course, *T* estimates from various thermometers need not match. The exchange of either Na or Ti between amphibole and liquid may have different closure temperatures; and no crystals form

isothermally. But when Eqns. (4-6) and (8-9) converge, some confidence in *T* estimates would appear warranted.

Finally, the present collection of experimental data also yield a simple model for the prediction of SiO_2 in co-existing liquid, which may be used in addition to Eqn. (2) as a test of equilibrium:

$$SiO_2 \text{ (wt. \%)} = 751.95 - 0.4T(^{o}C) - 278000/T(^{o}C) - 9.184[Al^{T\text{-amph}}] \quad (10)$$

Equation (10) recovers SiO_2 to ± 3.6 wt. %, with $R^2 = 0.86$ (n = 152). Below, we use Eqn. (10), in combination with (2), to check whether a given amphibole is correctly matched (equilibrated) with a given putative liquid composition.

IMPLICATIONS

Estimating Crystallization Pressures

The *P-T* conditions at which magmas partially crystallize before eruption can tell us much about magma transport, and possibly even eruption mechanisms. To illustrate, *P-T* estimates are obtained for two recent eruptions at subduction-related volcanoes: Merapi and Augustine. These examples show how amphibole *P-T* estimates (using Eqns. 7a, b; Eqns. 4, 9), can be combined with cpx-derived *P-T* conditions (using Putirka 2008), to better understand volcanic systems.

At Augustine Volcano (Tappen et al., 2009), and the 2010 eruption at Merapi (Erdman et al. 2014; Costa et al. 2013), magmas appear to be co-saturated with amphibole (amph), and clinopyroxene (cpx). In both cases, mixing lines between reported glass/matrix, whole rock (pumice) and mineral compositions are used to obtain liquids that achieve Fe-Mg exchange equilibrium between a putative liquid and a reported amph (Eqn. 2) or cpx

(see Putirka 2008) composition; for amph, we also check that putative liquids have SiO_2 contents within ~1σ to 1.5 σ of those SiO_2 predicted from Eqn. (10). Pressure-*T* estimates are derived from these mineral-liquid pairs, assuming the liquids contain 5 wt. % H_2O at both volcanoes. Amphibole *P* estimates (Eqn. (7a,b)) are sensitive to this assumption, increasing at a rate of 0.4 kbar per 1 wt.% increase in H_2O; amphibole thermometers, meanwhile, are effectively insensitive to H_2O (with <2°C change per 1 wt. % H_2O).

Both Augustine and Merapi show why a statistical approach, and independent tests of *P* and *T* are important, and for different reasons. At Augustine, cpx precipitates just near1100 °C at *P* = 5.7 to -1.8 kbar (the latter is not shown, but is within model error of 1 atm, so should not be discarded) (Fig. 9). The highest *P*, 5.7 kbar, derived from one cpx grain, may indicate deep-seated crystallization. The remaining cpx *P* estimates are identical within error, and yield a mean of $P \approx 0.6 \pm 1.9$ kbar. This nicely match estimates from five amphiboles, which yield a mean *P* of 0.9 ± 0.6 kbar (Eqn. 7a; H_2O = 5 wt. %). Interestingly, a lone Augustine amphibole also yields *P*=6.3 kbar—overlapping the high *P* cpx estimate within error. All Augustine amphiboles yield lower crystallization temperatures: 831±3°C at low *P*, and 979°C at 6.3 kbar. One Augustine amph yields *T* = 608°C, and is discarded, since this *T* is lower than Fe-Ti oxide temperatures (796±6°C; Tappen et al. 2009). Augustine cpx and amph grains thus paint a picture of mostly low *P* (~0.75 kbar) crystallization, with 270°C of cooling, from ~1100°C down to 830°C, but also some magma stagnation and cooling at about 6 kbar.

For the 2010 Merapi eruption (Erdman et al. 2014; Costa et al. 2013; Innocenti et al 2013), thermometry appears straightforward, but barometry is more challenging. Using Eqn. (10), we find that all but Type M1 megacrysts of Erdman et al. (2014) precipitate

from liquids with 57-64% SiO_2, while M1 crystals derive from a more mafic liquid, with 52-54% SiO_2. Using Eqns. (4a, b), all amphiboles, including M1 crystals, yield similar temperatures of 943±16ºC. Equations (5-6) yield higher temperatures for M1 crystals, of 976±9ºC, compared to 938±23ºC for the remaining amphiboles, but amphibole saturation temperatures are similar for all liquids, averaging 942±4ºC (Eqn. 3). The remarkably close agreement of the various thermometers indicates that Merapi amphiboles probably crystallized near 945±30 ºC, although perhaps as high 975ºC for M1 megacrysts.

But at what pressure? Clinopyroxene crystals (Costa et al. 2013) approach Fe-Mg exchange equilibrium with mafic liquids (Innocenti et al. 2013), and yield pressures of 0.8 to 4.3 kbar (avg. = 2.4±1.7 kbar) at 1131±27ºC. But amphibole *P* estimates are mostly greater, and the various models disagree (Fig. 9): excluding Type M1 crystals, Eqns. (7a) and (7b) yield 5.5±0.8, and 3.3±0.8 kbar respectively, while for M1 crystals, *P* is >5.8 kbar for all models.

The meaning of these amph *P* estimates at Merapi is unclear in the absence of cpx pressure estimates. Clinopyroxene is calculated to precede amph saturation by ~170-190ºC. This result is consistent experimental phase relationships (e.g., Grove et al. 2003; and Rutherford and Devine 2003), which indicate a minimum thermal interval of 100ºC between cpx and amph saturation, except at *P*<1 kbar. It thus seems unlikely that amph would crystallize at *greater P*, *and* at *lower T*. So if cpx and amph are magmatically related, then cpx barometry places a maximum *P* of 4.3 kbar for Merapi (2010 eruption) amphiboles, and thus only Eqn. 7b provides plausible estimates.

Another possibility is that the cpx and amph are not magmatically related, or that our assumed H_2O contents (5 wt. %) are incorrect. If amph and cpx are not magmatically

related, then the higher amph *P* estimates could be valid if amphiboles belong to older, cooler gabbroic precipitates, dredged up by the later 2010 magmas. But this then yields two problems of its own: (a) that similarly old, cold, deep cpx crystals were strangely not assimilated into the 2010 magmas (or the hypothetical deep gabbros were not cpx saturated, despite reaching amph saturation), and (b) that the 2010 Merapi magmas did not reach amph saturation at $P<4$ kbar (following cpx saturation), despite reaching Fe-Ti oxide saturation (Costa et al. 2013). But water contents could well be lower. Ghiroso (1999) shows that water saturated or near-saturated conditions need not represent the typical water contents in the *T* intervals over which liquids are saturated with amphibole. If H_2O is 2 wt. % then Eqns. 7a and 7b yield *P* estimates (excluding M1 crystals) of 4.1±0.8 and 2.1±0.9 kbar respectively, the latter of which now come quite close to the mean cpx *P* estimates (the amph and cpx mean is 2.2 kbar). Equation 7b also yields 4.3±1.9 for Type M1 crystals, (while Eqn. 7a yields $P = 7.8\pm2.3$ kbar for M1 crystals). Here, the lower water contents (2 wt. %) at Merapi may be sensible, given that amphibole *T* estimates are higher at Merapi than at Augustine.

In combination, the cpx and amph models indicate about 190-270ºC of cooling at ~1-2.2 kbar, although clearly, a more comprehensive examination of crystal compositions is needed. The finding that natural amphiboles consist of just a few components can guide further development of models such as MELTS (e.g., Ghiorso et al., 1995). To bolster such works, an urgent goal should be to explore natural amphibole components in detail with regard to their crystallographic and calorimetric properties, and to produce new partial melting experiments focused on amphibole saturation conditions.

Implications for Eruption Mechanisms

The import of the Augustine and Merapi *P-T* analysis is that irrespective of problems in amph *P* estimation, these systems undergo ~190-270ºC cooling at mostly shallow depths (≤2.2 kbar). This further implies that the influx of recharge magma is not the proximal cause of the eruptions in question. Recharge of mafic magma into a shallow felsic magma body may indeed rejuvenate stalled felsic magmas (e.g., see Klemetti and Clynne, 2014 for a well-documented case). But that influx is not a sufficient cause for eruption, even though some *P* increase may accompany the event (Blake, 1981). Instead, as long-ago postulated by Daly (1911), vapor saturation would appear to be the proximal eruptive trigger, providing the buoyancy needed to force magma to the surface. Recharge and heating at Merapi and Augustine are followed by minimum cooling intervals of 190ºC (Merapi, 2010) to 270ºC (Augustine)—a thermal cycle that is probably interrupted upon vapor saturation and eruption (see Jaupart and Tait 1990).

ACKNOWLEDGEMENTS

Sincere thanks are extended to Lawford Anderson and an anonymous reviewer, and Associate Editor Renat Almeev. All three provided very insightful and critical reviews that greatly improved the final product. The AE and the anonymous reviewer had very perceptive comments regarding details of several models, and the use of water as an independent variable, while Anderson urged for a more clear test of earlier Al-in-hornblende calibrations. All these comments led to improvements in testing procedures. I also thank the AE for introducing me to the Na-K exchange thermometer of Helz (1979), which proved to yield a remarkably precise means of predicting *T* in the global experimental database. Finally, I thank the National Science Foundation for their generous support. This work grew out of two broadly related projects funded by NSF, 1250322 and 1250323.

REFERENCES CITED

Adam, J., and Green, T.H. (1994) The effects of pressure and temperature on the partitioning of Ti, Sr and REE between amphibole, clinopyroxene and basanitic melts. Chemical Geology, 117, 219–233.

Adam, J., and Green, T. (2006) Trace element partitioning between mica- and amphibole-bearing garnet lherzolite and hydrous basanitic melt: 1. Experimental results and the investigation of controls on partitioning behavior. Contributions to Mineralogy and Petrology, 152, 1-17.

Adam, J., Green, T.H., Sie, S.H. (1993) Proton microprobe determined partitioning of Rb, Sr, Ba, Y, Zr, Nb and Ta between experimentally produced amphiboles and silicate melts with variable F content. Chemical Geology, 109, 29–49.

Adam, J., Oberti, R., Ca´mara, F., and Green, T.H. (2007) An electron microprobe, LAM-ICP-MS and single-crystal X-ray structure refinement study of the effect of pressure, melt-H_2O concentration and fO_2 on experimentally produced basaltic amphiboles. European Journal of Mineralogy, 19, 641–655.

Ague, J.J. and Brimhall, G.H. (1988) Regional variations in bulk chemistry, mineralogy, and the compositions of mafic and accessory minerals in the batholiths of California. Geological Society of America Bulletin, 100, 891-911.

Allen, J. C. and Boettcher, A. L. (1978) Amphiboles in andesite and basalt: II. Stability as a function of P-T-f_{H2O}-f_{O2},. American Mineralogist, 63, 1074-1087.

Almeev, R.R., Ariskin, A.A., Ozerov, A.Y., and Kononkova, N.N. (2002) Problems of the stoichiometry and thermobarometry of magmatic amphiboles: An example of hornblende from the andesites of Bezymianny volcano, Eastern Kamchatka. Geochemistry International, 40, 723-38.

Alonso-Perez R, Müntener O, Ulmer P (2009) Igneous garnet and amphibole fractionation in the roots of island arcs: experimental constraints on andesitic liquids. Contributions to Mineralogy and Petrology, 157:541–558.

Anderson, J.L. (1996) Status of thermobarometry in granitic batholihts. Transactions of the Royal Society of Edinburgh: Earth Sciences, 87, 125-138.

Anderson, J.L., Barth, A.P., Wooden, J.L., and Mazdab, F. (2008) Thermometers and thermobarometers in granitic systems. In Putirka, K.P. and Tepley, eds., Minerals, Inclusions and Volcanic Processes, Reviews in Mineralogy and Geochemistry v. 69, 121-142.

Anderson, J.L. and Smith, D.R. (1995) The effects of temperature and f_{O2} on the Al-in-hornblende barometer. American Mineralogist, 80, 549-599.

Barclay, J. and Rutherford, M.J. and Carroll, M.R. (1998) Experimental phase equilibria constraints on pre-eruptive storage conditions at Soufriere Hills magma. Geophysical Research Letters, 25, 3437-3440.

Barclay, J., and Carmichael, I.S.E. (2004) A hornblende basalt from western Mexico: water saturated phase relations constrain a pressure-temperature window of eruptibility. Journal of Petrology, 45, 485-506.

Barnes, C. G., Frost, C.F., Nordgulen, O. and Prestvik, T. (2012) Magma hybridization in the middle crust: possible consequences for deep-crustal magma mixing. Geosphere, 8, 518-533.

Berndt, J., Holtz, F., and Koepke, J. (2001) Experimental constraints on storage conditions in the chemically zoned phonolitic magma chamber of the Laacher See volcano. Contributions to Mineralogy and Petrology, 140, 469-486.

Blake, S. (1981) Volcanism and the dynamics of open magma chambers. Nature, 289, 783-785.

Blatter, D.L, and Carmichael, I.S.E. (2001) Hydrous phase equilibria of a Mexican high-silica andesite: A candidate for a mantle origin? Geochimica et Cosmochimica Acta, 65, 4043-4065.

Blundy, J.D., and Holland, T.J.B. (1990) Calcic amphibole equilibria and a new amphibole-plagioclase geothermometer. Contributions to Mineralogy and Petrology, 104, 208-224.

Botcharnikov, R.E., Holtz, F., Almeev, R.R., Sato, H., and Behrens, H. (2008) Storage conditions and evolution of andesitic magma prior to the 1991-95 eruption of Unzen volcano: constraints from natural samples and phase equilibria experiments. Journal of Volcanology and Geothermal Research, 175, 168-180.

Daly, R.A. (1911) The nature of volcanic action. Proceedings of the American Academy of Arts and Sciences, 47, 47-122.

Caricchi, L., Ulmer ,P. and Peccerillo, A. (2006) A high-pressure experimental study on the evolution of the silicic magmatism of the Main Ethiopian Rift. Lithos 91, 46–58.

Carroll, M.R., and Wyllie, P.J. (1989) Experimental phase relations in the system tonalite-peridotite-H_2O. Implications for assimilation and differentiation processes near the c rust-mantle boundary, Journal of Petrology, 30, 135, 1-1382.

Castro A. and Gerya T. V. (2008) Magmatic implications of mantle wedge plumes: Experimental study. Lithos, 103:138-148.

Coldwell, B., Adam, J., Rushmer, T., and Macpherson, C.G. (2011) Evolution of the East Philippine Arc: experimental constraints on magmatic phase relations and adakitic melt formation. Contributions to Mineralogy and Petrology, 162, 835-848.

Costa, F., Scaillet, B., Pichavant, M. (2004) Petrological and experimental constraints on the pre-eruption compositions of Holocene dacite from Volca`n San Pedro (36º S, Chilean Andes) and importance of sulphur in silicic subduction-related magmas. Journal of Petrology, 45, 855–881.

Costa, F., Andreastuti, S., de Maisonneuve, C.B., and Pallister, J.S. (2013) Petrological insights into the storage conditions, and magmatic processes that yielded the centennial 2010 Merapi explosive eruption. Journal of Volcanology and Geothermal Research, 261, 209-235.

Dalpe, C. and Baker, D.R. (1994). Partition coefficients for rare-earth elements between calcic amphibole and Ti-rich basanitic glass at 1.5 GPa, 1100 degrees C. Mineralogical Magazine, 58, 207-208.

Di Carlo, I., Rotolo, S.G., Scaillet, B., Buccheri, V., and Pichavant, M. (2010) Phase equilibrium constraints on pre-eruptive conditions of recent felsic explosive volcanism at Pantelleria Island, Italy. Journal of Petrology, 51, 2245-2276.

Dyar, M.D., McGuire, A.V., and Mackwell, S.J. (1992) Fe3+/H+ and D/H in kaersutites: misleading indicators of mantle source fugacities. Geology, 20, 565-568.

Dyar, M.D., Mackwell, S.J., McGuire, A.V., Cross L.R., and Robertson, J.D. (1993) Crystal chemistry of Fe^{3+} and H^{+} in mantle kaersutite: Implications for mantle metasomatism. American Mineralogist, 78, 968-979.

Erdman, S., Martel, C., Pichavant, M., and Kushnir, A. (2014) Amphibole as an archivist of magmatic crystallization conditions: problems, potential, and implications for inferring magma storage prior to the paroxysmal 2010 eruption of Mount Merapi, Indonesia. Contributions to Mineralogy and Petrology, doi 10.1007/s00410-014-1016-4.

Ernst, W.G. and Liu, J. (1998) Experimental phase-equilibrium study of Al- and Ti-contents of calcic amphibole in MORB – a semiquantitative thermobarometer. American Mineralogist, 83, 952–969.

Feig, S.T., Koepke, J., and Snow, J.E. (2010) Effect of oxygen fugacity and water on phase equilibria of a hydrous tholeiitic basalt. Contributions to Mineralogy and Petrology, 160, 551-568.

Foden, J. D. & Green, G. H. (1992) Possible role of amphibole in the origin of andesite: some experimental and natural evidence. Contributions to Mineralogy and Petrology 109, 479–493.

Freise, M., Holtz, F., Nowak, M., Scoates, J.S., and Strauss, H. (2009) Differentiation and crystallization conditions of basalts from the Kerguelen large igneous province: an experimental study. Contributions to Mineralogy and Petrology, 158, 505–527.

Gardien, V., Thompson, A.B., and Ulmer, P. (2000) Melting of biotite plus plagioclase plus quartz gneisses: the role of H_2O in the stability of amphibole. Journal of Petrology, 41, 651-666.

Gardner, J.E., Rutherford, M., Carey, S., and Sigurdsson, H. (1995) Experimental constraints on pre-eruptive water contents and changing magma storage prior to explosive eruptions of Mount St Helens volcano. Bulletin of Volcanology, 57, 1-17.

Ghiorso, M.S. (1999) On the stability relations of hydrous minerals in water-undersaturated magmas. American Mineralogist, 84, 1506-11.

Ghiorso, M. S. and Sack, R. O. (1995) Chemical mass transfer in magmatic processes IV. A revised and internally consistent thermodynamic model for the interpolation and extrapolation of liquid–solid equilibria in magmatic systems at elevated temperatures and pressures. Contributions to Mineralogy and Petrology, 119, 197–212.

Grove, T.L., Elkins-Tanton, L.T., Parman, S.W., Chatterjee, N., Müntener, O., and Gaetani, G.A. (2003) Fractional crystallization and mantle-melting controls on calc-alkaline differentiation trends. Contributions to Mineralogy and Petrology, 145, 515-533.

Grove, T.L., Donnelly-Nolan, J.M. and Housh, T. (1997) Magmatic processes that generated the rhyolite of Glass Mountain, Medicine lake volcano, N. California. Contributions to Mineralogy and Petrology, 127, 205-223.

Hawthorne, F.C. (1983) Crystal chemistry of the amphiboles. Canadian Mineralogist, 21, 173-480.

Hawthorne, F.C. (2012) A bond-topological approach to theoretical mineralogy: crystal structure, chemical composition and chemical reactions. Physics and Chemistry of Minerals, 39, 841-874.

Hammerstrom, J.M. and Zen, E. (1986) Aluminum in hornblende: an empirical igneous geobarometer. American Mineralogist, 71, 1297-1313.

Helz, R.T. (1976) Phase relations of basalts in their melting ranges at P_{H2O}=5kb. part II. melt compositions. Journal of Petrology, 17, 139-193

Helz, R.T. (1979) Alkali exchange between hornblende and melt: a temperature-sensitive reaction. American Mineralogist, 64, 953-965.

Hilyard, M., Nielsen, R.L., Beard, J.S., Patino-Douce, A., and Blencoe, J. (2000) Experimental determination of the partitioning behavior of rare earth and high field strength elements between pargasitic amphibole and natural silicate melts. Geochimica et Cosmochimica Acta, 64, 1103-1120.

Hirschmann, M. M., Ghiorso, M. S., Davis, F. A., Gordon, S. M., Mukherjee, S., Grove, T. L., Krawczynski, M., Medard, E. & Till, C. B. (2008). Library of experimental phase relations (LEPR): a database and web portal for experimental magmatic phase equilibria data. Geochemistry, Geophysics, Geosystems 9, Q03011, doi:10.1029/2007GC001894.

Holland, T.J.B., and Powell, R. (1998) An internally consistent thermodynamic data set for phases of petrological interest. Journal of Metamorphic Geology, 16, 309-343.

Hollister, L.S., Grissom, G.C., Peters, E.K., Stowell, H.H., and Sisson, V.B. (1987) Confirmation of the empirical correlation of Al in hornblende with pressure of solidification of calc-alkaline plutons. American Mineralogist, 72, 231-239.

Innocenti, S., del Marmol, M-A., Voight, B., Andreastuti, S., and Furman, T. (2013) Textural and mineral chemistry constraints on evolution of Merapi Volcano, Indonesia. Journal of Volcanology and Geothermal Research, 261, 20-37.

Irving, A.J. and Green, D.H. (2008) Phase relationships of hydrous alkali magmas at high pressures: production of nepheline hawaiitic to mugearitic liquids by amphibole-dominated fractional crystallization within the lithospheric mantle. Journal of Petrology, 49, 741–756.

Holtz, F., Sato, H,, Lewis, J., Behrens, H., Nakada, S. (2005) Experimental Petrology of the 1991-19995 Unzen Dacite, Japan. Part I: Phase relations, phase composition, and pre-eruptive conditions. Journal of Petrology 46, 319-337.

Irving, A.J., Green, D.H. (2008) Phase relationships of hydrous alkali magmas at high pressures: production of nepheline hawaiitic to mugearitic liquids by amphibole dominated fractional crystallization within the lithospheric mantle. Journal of Petrology, 49, 741–756.

Jaupart, C. and Tait, S. (1990) Dynamics of eruptive phenomena. In, Modern Methods of Igneous Petrology: Understanding Magmatic Processes, J. Nicholls & J. K. Russell, eds., Reviews in Mineralogy and Geochemistry. 24, 213-238.

Johnson, M.C., and Rutherford, M.J. (1989) Experimental calibration of an aluminum-in-hornblende geobarometer applicable to calc-alkaline rocks. EOS, 69, 1511.

Johnson, M.C., and Rutherford, M.J. (1989) Experimental calibration of an aluminum-in-hornblende geobarometer applicable to Long Valley caldera (California) volcanic rocks. Geology, 17, 837-841.

Kaszuba, J.P. and Wendlandt, R.F. (2000) Effect of carbon dioxide on dehydration melting reactions and melt compositions in the lower crust and the origin of alkaline rocks. Journal of Petrology, 41, 363–386.

Kawamoto, T. (1996) Experimental constraints on differentiation and H_2O abundance of calc-alkaline magmas. Earth and Planetary Science Letters, 144:577–589.

King, P.L., Hervig, R.L., Holloway, J.R., Delaney, J.S., and Dyar, M.D. (2000)

Partitioning of Fe^{3+}/Fe_{total} between amphibole and basanitic melt as a function of oxygen fugacity. Earth and Planetary Science Letters, 178, 97-112.

Klein, M., Stosch, H.G. and Seck, H.A. (1997) Partitioning of high field-strength and rare-earth elements between amphibole and quartz-dioritic to tonalitic melts: An experimental study. Chemical Geology 138, 257-271.

Klemetti, E.K., and Clynne, M.A. (2014) Localized rejuvenation of a crystal mush recorded in zircon temporal and compositional variation at the Lassen Volcanic Center, Northern California. PLoS ONE 9, doi:10.1371/journal.pone.0113157.

Koepke, J., Berndt, J., Bussy, F. (2003) An experimental study on the shallow-level migmatization of ferrogabbros from the Fuerteventura Basal Complex, Canary Islands. Lithos, 69, 105–125.

Koester, E., Pawley, A.R., Fernandes, L.A., Porcher, C.C., Soliani, Jr. E. (2002) Experimental melting of cordierite gneiss and the petrogenesis of syntranscurrent peraluminous granites in southern Brazil. Journal of Petrology, 43, 1595-1616.

Krawczynski, M.J., Grove, T.L. and Behrens, H. (2012) Amphibole stability in primitive arc magmas : effects of temperature, H_2O content and oxygen fugacity. Contributions to Mineralogy and Petrology, 164, 317-339.

Lange, R. L. & Carmichael, I. S. E. (1990) Thermodynamic properties of silicate liquids with emphasis on density, thermal expansion and compressibility. In: Nicholls, J. & Russell, J. K. (eds) Modern Methods of Igneous Petrology. Mineralogical Society of America, Reviews in Mineralogy 24, 25-64.

Leake, B.E., Woolley, A.R., Arps, C.E.S., Birch, W.D., Gilbert, M.C., Grice, J.D., Hawthorne, F.C., Kato, A., Kisch, H.J., Krivovichev, V.G., Linthout, K., Laird, J., Mandarino, J.A., Maresch, W.V., Nickel, E.H., Rock, N.M.S., Schumacher, J.C., Smith, D.C., Stephenson, N.C.N., Ungaretti, L., Whittiker, E.J.W., and Youzhi, G. (1997) Nomenclature of amphiboles: report of the subcommittee on amphiboles of the International Mineralogical Association, Commission on New Minerals and Mineral Names. Canadian Mineralogist, 35, 219-246.

Mahood, G.A. and Baker, D.R. (1986) Experimental constraints on depths of fractionation of mildly alkalic basalts and associated felsic rocks: Pantelleria, Strait of Sicily. Contributions to Mineralogy and Petrology, 93, 251-264.

Maksimov, A.P. (2009) The influence of water on the temperature of amphibole stability in melts. Journal of Volcanology and Seismology, 3, 27–33.

Martel, C., Pichavant, M., Holtz, F., Scaillet, B., Bourdier, J.L., Traineau, H. (1999) Effects of fO_2 and H_2O on andesite phase relation between 2 and 4 kbar. Journal of Geophysical Research, 104, 29453–29470.

McCanta, M.C., Rutherford, M.J., Hammer, J.E. (2007) Pre-eruptive and syn-eruptive conditions in the Black Butte, California dacite: Insight into crystallization kinetics in a silicic magma system. Journal of Volcanology and Geothermal Research, 160, 263–284.

Mercer, C. and Johnston, A.D. (2008) Experimental studies of the P–T–H_2O near-liquidus phase relations of basaltic andesite from North Sister Volcano, High Oregon Cascades: constraints on lower-crustal mineral assemblages. Contributions to Mineralogy and Petrology, 155, 571–592.

Molina, J.F., Moreno, J.A., Castro, A., Rodruiguez, C., and Fershtater, G.B. (2015) Calcic amphibole thermobarometry in metamorphic and igneous rocks: new

calibrations based on plagioclase/amphibole Al-Si partitioning and amphibole-liquid Mg partitioning. Lithos, 232, 286-305.

Moore, G. and Carmichael, I.S.E. (1998) The hydrous phase equilibria (to 3 kbar) of an andesite and basaltic andesite from western Mexico: constraints on water content and conditions of phenocryst growth. Contributions to Mineralogy and Petrology, 130, 304–319.

Müntener, O., Kelemen, P.B., Grove, T.L. (2001) The role of H_2O during crystallization of primitive arc magmas under uppermost mantle conditions and genesis of igneous pyroxenites: and experimental study. Contributions to Mineralogy and Petrology, 141, 643-658.

Naney, M. T. (1983) Phase equilibria of rock forming ferromagnesian silicates in granitic systems. American Journal of Science, 283, 993–1033.

Nekvasil, H., Dondolini, A., Horn, J., Filiberto, J., Long, H., and Lindsley, D.H. (2004) The origin and evolution of silica-saturated alkalic suites: an experimental study. Journal of Petrology, 45,693–721.

Patino-Douce, A.E. and Beard, J.S. (1995) Dehydration-melting of biotite gneiss and quartz amphibolite from 3 to 15 kbar. Journal of Petrology, 36, 707-738.

Pichavant, M., Martel, C., Bourdier, J.L., Scaillet, B. (2002) Physical conditions, structure, and dynamics of a zoned magma chamber: Mount Pelee` (Martinique, Lesser Antilles Arc). Journal of Geophysical Research, 107, 2093. doi:10.1029/2001JB000315

Pietranik, A., Holtz, F., Koepke, J., Puziewicz, J. (2009) Crystallization of quartz dioritic magmas at 2 and 1 kbar: experimental results. Mineralogy and Petrology, 97, 1–21.

Pickett, D.A., and Saleeby, J.B. (1993) Thermobarometric constraints on the depth of exposure and conditions of plutonism and metamorphism at deep levels of the Sierra Nevada Batholith, Tehachipi Mountains, California. Journal of Geophysical Research, 98, 609-629.

Pilet, S., Ulmer, P., Villiger, S. (2010) Liquid line of descent of a basanitic liquid at 1.5 GPa: constraints on the formation of metasomatic veins. Contributions to Mineralogy and Petrology, 159, 621–643.

Prouteau, G. and Scaillet, B. (2003) Experimental constraints on the origin of the 1991 Pinatubo dacite. Journal of Petrology, 44, 2203–2241.

Prouteau, G., Scaillet, B. Pichavant, M., and Maury, R.C. (1999) Fluid-present melting of ocean crust in subduction zones. Geology, 27, 1111-1114.

Putirka, K. D. (2008) Thermometers and barometers for volcanic systems, in: Putirka, K. D., and Tepley, F. eds., Reviews in Mineralogy and Geochemistry, 69, p. 61-120.

Putirka, K., M. Johnson, R. Kinzler, and D. Walker (1996) Thermobarometry of mafic igneous rocks based on clinopyroxene-liquid equilibria, 0-30 kbar, Contributions to Mineralogy and Petrology, v. 123, p. 92-108.

Putirka, K., Ryerson, F. J., and Mikaelian, H. (2003) New igneous thermobarometers for mafic and evolved lava compositions, based on clinopyroxene + liquid equilibria, American Mineralogist, v. 88, p. 1542-1554.

Rapp, R.P., and Watson, E.B. (1995) Dehydration melting of metabasalt at 8–32 kbar: Implications for continental growth and crust-mantle recycling: Journal of Petrology, 36, 891–931.

Ridolfi, F., and Renzulli, A. (2011) Calcic amphiboles in calc-alkaline and alkaline

magmas: thermobarometric and chemometric empirical equations valid up to 1,130ºC and 2.2 GPa. Contributions to Mineralogy and Petrology, doi: 10.1007/s00410-011-0704-6.

Rutherford, M.J., and Devine, J.D. (2003) Magmatic conditions of magma ascent as indicated by hornblende phase equilibria and reactions in the 1995-2002 Soufriere Hills Magma. Journal of Petrology, 44, 1433-1454.

Sato, H., Nakada, S., Fujii, T., Nakamura, M., and Suzuki-Kamata, K. (1999) Groundmass pargasite in the 1991-1995 dacite of Unzen volcano: phase stability experiments and volcanological implications. Journal of Volcanology and Geothermal Research, 89, 197-212.

Sato, H., Holtz, F., Beherens, H., Botcharnikov, R., and Nakada, S. (2005) Experimental petrology of the 1991–1995 Unzen Dacite, Japan. Part II: Cl/OH partitioning between hornblende and melt and its implications for the origin of oscillatory zoning of hornblende phenocrysts. Journal of Petrology, 42, 339–354.

Scaillet, B. and Evans, B.W. (1999) The 15 June 1991 Eruption of Mount Pinatubo. I. Phase Equilibria and pre-eruption P-T-fO_2-fH_2O conditions of the dacite magma. Journal of Petrology, 40, 381-411.

Scaillet, B. and MacDonald, R. (2003) Experimental constraints on the relationships between peralkaline rhyolites of the Kenya rift valley. Journal of Petrology, 44, 1867-1894.

Schmidt, M.W. (1992) Amphibole composition in tonalite as a function of pressure: an experimental calibration of the Al-in-hornblende barometer. Contributions to Mineralogy and Petrology, 110, 304-310.

Scoates, J.S., Lo Cascio, M., Weis, D., and Lindsley, D.H. (2006) Experimental constraints on the origin and evolution of mildly alkalic basalts from the Kerguelen Archipelago, Southeast Indian Ocean. Contributions to Mineralogy and Petrology, 151, 582-599.

Sisson, T.W., Grove, T.L. (1993) Experimental investigations of the role of H_2O in calc-alkaline differentiation and subduction zone magmatism. Contributions to Mineralogy and Petrology, 113, 143-166

Sisson, T., Ratajeski, K., Hankins, W., Glazner, A. (2005) Voluminous granitic magmas from common basaltic sources. Contributions to Mineralogy and Petrology 148, 635–661.

Skjerlie, K.P., Johnston, A.D. (1996) Vapour-absent melting from 10 to 20 kbar of crustal rocks that contain multiple hydrous phases: implications for anatexis in the deep to very deep continental crust and active continental margins. Journal of Petrology 37, 661–691.

Springer, W. and Seck, H.A. (1997) Partial fusion of basic granulites at 5 to 15 kbar: implications for the origin of TTG magmas. Contributions to Mineralogy and Petrology, 127, 30-45.

Thompson, J.B. (1982) Composition space: an algebraic and geometric approach. *In*: Characterization of Metamorphism Through Mineral Equilibria. Ferry, J.M., ed., p 1-31.

Tappen, C.M., Webster, J.D., Mandeville, C.W., and Roderick, D. (2009) Petrology and

geochemistry of ca. 2100-1000 a B.P. magmas of Augustine volcano, Alaska, based on analysis of prehistoric pumicious tephra. Journal of Volcanology and Geothermal Research, 183, 42-62.

Tomiya, A., Takahashi, E., Furukawa, N., and Suzuki, T. (2010) Depth and evolution of a silicic magma chamber: melting experiments on a low-K rhyolite from Usu Volcano, Japan. Journal of Petrology, 51, 1333-1354.

Popp, R.K., Virgo, D., Yoder, H.S., Hoering, T.C., and Phillips, M.W. (1995) An experimental-study of phase equilibria and Fe oxy-component in kaersutitic amphibole—implications for the f(H2) and a(H2O) in the upper mantle. American Mineralogist, 80, 534-548.

Wolff, P.E., Koepke, J., and Feig, S.T. (2012) The reaction mechanisms of fluid-induced partial melting of gabbro in the oceanic crust. European Journal of Mineralogy, 25, 279-298.

Figure Captions

Figure 1. Calcic amphibole compositions from 573 partial melting experiments. Closed circles are amphiboles with <6 Si cations per formula unit (as shown later, these reveal a yet to be recognized amphibole component; see text). Total Al cations in amphibole (Al^T), on a 23 oxgyen basis, are compared to (a) pressure, (b) temperature, and (c) Al_2O_3 contents of equilibrated liquids. In (c), Mg-Fe-Mn-Li group amphbioles from DiCarlo wt al. (2010) and Scaillet and MacDonald (2003), with very low Al^T are shown. (d) compares D_{Al} against P/T; the slight increase in D_{Al} indicates that the partitioning of Al might be a weak barometer. (e) compares two Al-bearing amphibole-liquid equilibria: (1) pargasite-liquid: $0.5Na_2O^{liq} + 2CaO^{liq} + 4FmO^{liq} + 1.5Al_2O_3{}^{liq} + 6SiO_2 + H_2O^{liq} = NaCa_2(Fm_4Al)Si_6Al_2O_{22}(OH)_2$, and (2) Alumino-tschermakite-liquid: $2CaO^{liq} + 3FmO^{liq} + 2Al_2O_3{}^{liq} + 6SiO_2 + H_2O^{liq} = Ca_2(Fm_3Al_2)Si_6Al_2O_{22}(OH)_2$; neither of these vary systematically with P/T. Here, pargasite is taken as the number of Na cations in amphibole, while Al-tschermakite is ½ of all octahedrally coordinated Al, both calculated

on a 23 cation basis; all activities are ideal (equal to mole fractions). Other equilibria, components, involving for example various other Al(IV) and Al(VI) amphibole components are equally immune to changes in *P*/*T*. Data sources are listed in the caption to Fig. 5. (f) is the same as (d), but vertical axis is extended downward to 0.5, to show the location of Mg-Fe-Mn-Li group amphiboles in (c).

Figure 2. Al^T vs. Si (atoms per formula unit, or apfu) for experimental data (calcic amphiboles, on the basis of Leake et al. 1994) divided on the basis of (a) pressure (2 kbar intervals) and (b) temperature (~80 ºC intervals). Those data with Al^T<0.75 and Si>7.5 are Mg-Fe-Mn-Li group amphiboles from DiCarlo wt al. (2010) and Scaillet and MacDonald (2003), which are used as test data. Panel (a) shows that low pressure experiments (0 – 1.9 kbar) yield equivalently high Al and low Si contents in amphiboles compared to experiments performed at 8 – 10 kbar, while (b) shows a progressive increase in mean Al^T and decrease in mean Si as temperature increases for the very same data.

Figure 3. (a) Al^T vs. Al(IV) and (b) Mg# (= $Mg^{amph}/(Mg^{amph} + Fe^{amph})$ vs. Si; all cations calculated on a 23 oxygen basis. Al(IV) = 8 – Si. The Al^{VI}/Al^T slope of 0.21 (Ridolfi and Renzulli (2011) is shown. Both charts show that most experimental data plot very similar to natural samples, thus providing a reasonable approximation to the processes that generate natural amphibole crystals. (c), (d) and (e) compare Na, Si and Al^T on a 23 oxygen basis, with end-member compositions as yellow triangles (in the formulas that follow, Fm = FeO + MgO): T-FA = Tremolite-Ferro-Actinolite = $Ca_2Fm_5Si_8O_{22}(OH)_2$;

Al-tsch = $Ca_2(Fm_3Al_2)Si_6Al_2O_{22}(OH)_2$; Na-Ged = Na-Gedrite, $NaFm_6AlSi_6Al_2O_{22}(OH)_2$; Parg = Pargasite, $NaCa_2(Fm_4Al)Si_6Al_2O_{22}(OH)_2$; K-Ged is K-Gedrite, $KFm_6AlSi_6Al_2O_{22}(OH)_2$; Kaers = Kaersutite, $NaCa_2(Fm_4Ti)Si_6Al_2O_{23}(OH)_2$; K-Ed = K-Edenite, $KCa_2Fm_5Si_7AlO_{22}(OH)_2$; Al-K = Aluminous kaersutite with the approximate composition of $NaCaFm_4Ti(Fe^{3+}, Al)Si_5Al_3O_{23}(OH)$. For natural samples, FmO = FeO + MgO + MnO. Note that nearly all compositions are encompassed by just a few components.

Figure 4. Ternary projections of experimental and natural amphibole compositions, using the exchange components of Tables 2A, B. In both panels, amphibole compositions are plotted using the Tremolite+Ferro-Actinolite (T-FA) and $NaAlSi_{-1}$ exchange parameters. Respectively, the upper and lower plots use the Kaersutite $NaTiAl_2Fm_{-1}Si_{-2}H_{-1}$, and KNa_{-1} exchange parameters. T-FA = $Ca_2Fm_5Si_8O_{22}(OH)_2$; Na-Ged = Na-Gedrite, $NaFm_6AlSi_6Al_2O_{22}(OH)_2$; Parg = Pargasite, $NaCa_2(Fm_4Al)Si_6Al_2O_{22}(OH)_2$; K-Ged = K-Gedrite, $KFm_6AlSi_6Al_2O_{22}(OH)_2$; Kaers = Kaersutite, $NaCa_2(Fm_4Ti)Si_6Al_2O_{23}(OH)_2$; K-Ed = K-Edenite, $KCa_2Fm_5Si_7AlO_{22}(OH)_2$. Both panels show that 1) experimental and natural compositions not only have similar compositions, but appear to exhibit the same stoichiometric substitutional mechanisms; 2) calcic igneous amphiboles can be described by just a handful of exchange parameters: they are mostly solid solutions of Tremolite-Ferro Actinolite + Pargasite + Kaersutite; a small fraction of very low Si amphiboles trend towards either a K- or Na-rich Gedrite. Adding Fe^{3+} to amphiboles changes the results not at all, and (not shown) Fe^{3+} variations (when $Fe^{3+}_{amph}/Fe^{2+}_{amph} = Fe^{3+}_{liq}/Fe^{2+}_{liq}$) can be explained using Ferri-ferrotschermakite, $Ca_2(Fm^{2+}_3Fe^{3+}_2)Si_6Al_2O_{22}(OH)_2$.

Figure 5. Tests of new and published thermometers. Standard errors of estimate (SEE) are the formal 1-sigma model (root mean square) error. Solid lines are 1-to-1 lines; deviations from such reflect both random and systematic error; slope and intercept values on regression lines (*T*(measured) vs. *T*(calculated)) measure systematic error, and should ideally be 1.0 and 0.0 respectively. (a) Ridolfi and Renzulli (2011), (b) Molina et al. (2015), their D_{Mg} thermometer, (c) Molina et al. (2015), their liquid only thermometer, (d) Eqn. (3), (e-f) Eqns. (4a) and (4b), and (g-h), Eqns. (5-6). The new calibrations are able to describe and predict *T* for a wider range of experimental observations, mostly with greater precision. DS1 = Data set 1 (n = 158) is used as a starting point for calibration and are from: Alonso-Perez et al. (2009), Barclay and Carmichael (2004), Costa et al. (2004), Dalpe and Baker (2000), Freise et al. (2009), Holtz et al. (2005), Moore and Carmichael (1998), Nekvasil et al. (2004), Pilet et al. (2010), Scaillet and Evans (1999), Sisson and Grove (1993). See Putirka (2008) for calibration methods. DS2 = Data set 2 are "test data", which comprises all experimental data not used for calibration (including data rejected from DS1); these are from: Helz (1976), Allen and Boettcher (1978), Naney (1983), Carroll and Wyllie (1989), Adam et al. (1993), Adam and Green (1994, 2006), Foden and Green (1992), Gardner et al. (1995), Patino-Douce and Beard (1995), Rapp (1995), Rapp and Watson (1995), Kawamoto (1996), Mahood and Baker (1996), Skjerlie and Johnston (1996), Grove et al. (1997), Klein et al. (1997), Springer and Seck (1997), Barclay et al. (1998), Ernst and Liu (1998), Prouteau et al. (1999), Gardien et al. (2000), Hilyard et al. (2000), Kaszuba and Wendlandt (2000), King et al. (2000), Berndt et al.

(2001), Blatter and Carmichael (2001), Müntener et al. (2001), Pichavant et al. (2002), Grove et al. (2003), Koepke et al. (2003), Prouteau and Scaillet (2003), Rutherford and Devine (2003), Scaillet and MacDonald (2003), Sato et al. (2005), Sisson et al. (2005), Caricchi et al. (2006), Scoates et al. (2006), McCanta et al. (2007), Botcharnikov et al. (2008), Castro et al. (2008), Irving and Green (2008), Mercer and Johnston (2008), Freise et al. (2009), Pietranik et al. (2009), DiCarlo et al. (2010), Feig et al. (2010), Tomiya et al. (2010), Coldwell et al. (2011), Krawczynski et al. (2012), Wolf et al. (2012).

Figure 6. (a) – (f): Tests of new and published barometers with data, statistics and 1-to-1 lines, as in Figure 5. Blue squares represent DS2, divided into isobaric sets (or nearly isobaric, where, for example, all experiments performed at <2 kbar are averaged together); here, the average of all calculated *P* estimates at a given *P* (over multiple studies and multiple bulk compositions) are compared to the reported (or average of reported) *P*. (a) Ridolfi and Renzulli (2011), model 1a; (b) Ridolfi and Renzulli (2011) model 1b; (c) Ridolfi and Renzulli (2011) model 1d (the best barometer from their study); (d) Eqn. (7a); (e) Eqn. (7b); (f) Eqn. (7c). In panels (g) to (j) are tests of select barometers using data DS3, which is comprised of data from DS1+DS2, with the restrictions that $T \leq 800^{o}C$ and $Fe\# = Fe^{amph}/(Fe^{amph}+Mg^{amph}) < 0.65$, from Anderson and Smith (1995). (g) Anderson and Smith (1995) barometer; (h) Hollister et al. (1987); (i) Ridolfi and Renzulli (2011) model 1d; (j) and Eqn. 7b. Although Eqn. 7a performs best at $P<10$ kbar for DS1 and DS2 (panels (a) – (f)), Eqn. (7b) is shown as it outperforms Eqn. 7a for DS3. Our calibration data set DS1 shows that it is possible to calibrate a barometer on a much larger data set compared to prior students. But when applied to predict P on individual

amphibole grains using DS2, *P* estimates are nearly useless for understanding crustal processes (SEE = ± 3.6 to 4.3 kbar), even for the newly calibrated models. However, mean experimental pressure estimates can be predicted, and all models are more precise and accurate at $T \leq 800^{o}C$ and Fe# <0.65 (see Anderson and Smith 1995).

Figure 7. Test of barometers on a study-by-study basis; solid lines are 1-to-1 lines. Plotted *P* estimates are obtained by averaging *P* estimates from multiple isobaric (or near isobaric) experiments from a given study. (a) Ridolfi and Renzulli (2011) model 1d, (b) and Eqn. (7a) and (c) Eqn. (7b). Regression statistics are for experiments conducted at $P \leq 8$ kbar; where H_2O contents are not measured, H_2O is estimated as 100 minus the anhydrous sum. Mean average pressures are calculated for: Sato et al. 1999 (< 2 kbar); Gardner et al. 1995 (1.5 kbar); Scaillet and McDonald 2003 (< 2 kbar); Botcharnikov et al. (2 kbar); Feig et al. 2010 (2 kbar); Sato et al. 2005 (2 kbar); Grove et al. 1997 (2 kbar); Wolf et al. 2012 (ca. 2 kbar); Sato et al.2005 (3 kbar); Pichavant et al. 2002 (ca. 4 kbar); Krawczynski et al. 2012 (5 kbar); Hilyard et al 2000 (5 kbar); Sisson et al. 2005 (7 kbar); Caricchi et al 2006 (7 kbar); Krawczynski et al. 2012 (8 kbar); Grove et al. 2003 (8 kbar); Prouteau and Scaillet 2003 (9-10 kbar); Klein et al 1997 (10 kbar); Patino-Douce and Beard 1995 (10 kbar); Foden and Green 1992 (10 kbar); Ernst and Liu 1998 (10 kbar); Grove et al 1997 (10 kbar). Clearly, only Eqn. (7b) can predict mean pressures with precision or accuracy.

Figure 8. Two thermometers, (a) Eqn. (8) which relies on amphibole compositions only, and (b) Eqn. (9), which uses the Na-K exchange (Helz 1979), are calibrated using all

available experimental data, where calcic-amphiboles are in equilibrium with liquid, irrespective of other conditions. Equation (9) also makes use of the Mg-Fe-Mn-Li amphiboles from DiCarlo et al. (2010) and Scaillet and MacDonald (2003). Statistical parameters illustrate how well *T* is recovered for the calibration data. Solid lines are 1-to-1 lines.

Figure 9. Clinopyroxene (diamonds) and amphibole (squares) *P-T* estimates for volcanic samples from Augustine Volcano (Tappen et al. 2009; dark gray) and Merapi (Erdman et al. 2014; light gray to white). While cpx and amph *P* estimates agree at Augustine, *P* estimates at Merapi are less clear; Merapi amph *P* estimates are only in agreement with cpx when applying Eqn. 7b, and by assuming H_2O = 2 wt. %. In any case, clinopyroxene precedes amph saturation, by ~190ºC (Merapi) and ~270ºC (Augustine). These results indicate that magma recharge is not the proximal cause of eruption. Rather, recharge is succeeded by crystallization and cooling prior to eruption, probably to the point of vapor saturation, which then triggers the final magmatic ascent.

Table 1. Comparison of molar volumes and the volume changes upon fusion of various amphibole and pyroxene components

Mineral-liquid equilibria	***Molar Volume (J/bar, 298 K)[1]***	***% ΔV (1273 K)[2]***
Grunerite; $Fe_7Si_8O_{22}(OH)_2$	27.8	13.1
Cummingtonite; $Mg_7Si_8O_{22}(OH)_2$	26.3	14.2
Tremolite; $Ca_2(Mg_5)Si_8O_{22}(OH)_2$	27.3	13.9
Ferroactinolite; $Ca_2(Fe_5)Si_8O_{22}(OH)_2$	28.3	13.4
Al-Tschermakite; $Ca_2(Mg_3Al_2)Si_6Al_2O_{22}(OH)_2$	26.8	15.0
Pargasite; $NaCa_2(Mg_4Al)Si_6Al_2O_{22}(OH)_2$	27.2	15.2
Jadeite; $NaAlSi_2O_6$	6.04	37.9
Diopside; $CaMgSi_2O_6$	6.62	17.8

1. Molar volume data are from Holland and Powell (1998)at 298K. 2. % ΔV are the percent volume changes upon fusion of the indicated mineral components at 1273 K, with liquid molar volumes calculated using Lange and Carmichael (1990) and using mineral thermal expansion coefficients from Holland and Powell (1998); for example, for Diopside, the % volume change is from the equilibrium: $CaMgSi_2O_6^{pyx} = CaO^{liq} + MgO^{liq} + 2SiO_2^{liq}$. Calculations are performed at 1273K so as to split the difference between expected saturation temperatures of pyroxene and amphibole in an intermediate composition magma, so as to compare pyroxenes and amphiboles under the same conditions.

1105 **Table 2.** Amphibole exchange components used for solid solution analysis

Amphibole Components & Exchange Parameters		*SiO_2*	*TiO_2*	*$AlO_{1.5}$*	*FeOt*	*MgO*	*CaO*	*$NaO_{1/2}$*	*$KO_{0.5}$*
Cummingtonite	$Mg_7Si_8O_{22}(OH)_2$	8	0	0	0	7	0	0	0
Tremolite	$Ca_2(Mg_5)Si_8O_{22}(OH)_2$	8	0	0	0	5	2	0	0
Kaersutite exchange	$NaTiAl_2Mg_{-1}Si_{-2}H_{-1}$	-2	1	2	0	-1	0	1	0
Na-K exchange	$Na_{-1}K$	0	0	0	0	0	0	-1	1
Al-Tschermakite exchange	$Al_4Si_{-2}Mg_{-2}$	-2	0	4	0	-2	0	0	0
NaAl-Si exchange	$NaAlSi_{-1}$	-1	0	1	0	0	0	1	0
Fe-Mg exchange	$Mg_{-1}Fe$	0	0	0	1	-1	0	0	0
Fictive	$Si_{11.5}O_{22}(OH)_2$	11.5	0	0	0	0	0	0	0

1106

1107 **Table 3**. Matrix used to convert cation fractions to amphibole exchange components

	Cummingtonite	*Tremolite*	*Kaersutite Exchange*	*Na-K exchange*	*Al-Tschermakite Exchange*	*NaAl-Si exchange*	*Fe-Mg exchange*	*Fictive*
	$Mg_7Si_8O_{22}(OH)_2$	$Ca_2(Mg_5)Si_8O_{22}(OH)_2$	$NaTiAl_2Mg_{-1}Si_{-2}H_{-1}$	$Na_{-1}K$	$Al_4Si_{-2}Mg_{-2}$	$NaAlSi_{-1}$	$Mg_{-1}Fe$	$Si_{11.5}O_{22}(OH)_2$
SiO_2	0	0	0	0	0	0	0	0.086956522
TiO_2	0.071428571	0	1	0	-0.25	-1	0	-0.00621118
$AlO_{1.5}$	0.071428571	0	0	0	0.25	0	0	-0.00621118
FeOt	0.142857143	0	0	0	0	0	1	-0.099378882
MgO	0.142857143	0	0	0	0	0	0	-0.099378882
CaO	-0.357142857	0.5	0	0	0	0	0	-0.099378882
$NaO_{1/2}$	-0.071428571	0	0	0	-0.25	1	0	0.093167702
$KO_{0.5}$	-0.071428571	0	0	1	-0.25	1	0	0.093167702

1108

Table 4a. Example of Amphibole Exchange Component Calculations

Weight % Amphibole (from Erdman et al. 2014)

	SiO_2	TiO_2	Al_2O_3	FeOt	MnO	MgO	CaO	Na_2O	K_2O	Cr	Sum
1)	42.2	2.75	11.1	13.1	0.39	13.55	11.07	2.27	0.95	0.01	97.39

Amphibole Cations on Basis of 23 O (1)

	Si	Ti	Al	Fe_{total}	Mg	Ca	Na	K	Sum
2)	6.28931	0.30829	1.94971	1.63274	3.01050	1.76771	0.65594	0.18062	15.79483

Amphibole cation fractions (renormalized without Mn or Cr) (2)

	Si	Ti	Al	Fe_{total}	Mg	Ca	Na	K	Sum (2)
3)	0.39819	0.01952	0.12344	0.10337	0.19060	0.11192	0.04153	0.01144	1

Amphibole Exchange Components (3)

	$Mg_7Si_8O_{22}(OH)_2$	$Ca_2(Mg_5)Si_8O_{22}(OH)_2$	$NaTiAl_2Mg_{-1}Si_{-2}H_{-1}$	$Na_{-1}K$	$Al_4Si_{-2}Mg_{-2}$	$NaAlSi_{-1}$	$Mg_{-1}Fe$	$Si_{11.5}O_{22}(OH)_2$	sum
4)	0.00845	0.05596	0.01952	0.01144	0.01274	0.03345	0.10337	-0.00167	0.24492

Amphibole Components – Renormalized (4)

	$Mg_7Si_8O_{22}(OH)_2$	$Ca_2(Mg_5)Si_8O_{22}(OH)_2$	$NaTiAl_2Mg_{-1}Si_{-2}H_{-1}$	$Na_{-1}K$	$Al_4Si_{-2}Mg_{-2}$	$NaAlSi_{-1}$	$Mg_{-1}Fe$	$Si_{11.5}O_{22}(OH)_2$	sum
5)	0.03452	0.22847	0.07969	0.04669	0.05201	0.13656	0.42206	0	1.00

(1) Cations on the basis of 23 oxygens (row 2), are derived from weight % oxides (row 1) as in Table 4b. (2) Amphibole cation fractions (row 3): calculated from the cations on a 23 oxygen basis (row 2), but leaving out Cr and Mn in the sum; so we have: Si + Ti + Al + Fe_{total} + Mg + Ca + Na + K = 1. (3) Amphibole exchange components (row 4): this is the product of the 8 x 1 row matrix (row 4) "Amphibole Cation Fractions", and the 8x 8 square matrix of Table 3. (4) The amphibole exchange components in row 5) are those as in row 4), but renormalized, ignoring $Si_{11.5}O_{22}(OH)_2$. If the components of Tables 2 and 3 are adequately describing a given amphibole, then the fictive component $Si_{11.5}O_{22}(OH)_2$ should be close to zero. This calculation scheme is neither a test of equilibrium, nor a test of whether a given amphibole composition is valid. If the component $Si_{11.5}O_{22}(OH)_2$ is not negligible, then the selected components might not be adequately describing a given composition.

Table 4b. Example of Amphibole Component Calculations

Merapi 2010 Amphibole, Type P1 (Erdman et al. 2014)

Weight %

	SiO_2	TiO_2	Al_2O_3	FeO_{total}	MnO	MgO	CaO	Na_2O	K_2O	sum
1)	40.570	2.450	12.820	13.110	0.260	13.020	11.630	2.200	0.920	96.98
	Mole proportions									
2)	0.675	0.031	0.126	0.182	0.004	0.323	0.207	0.035	0.010	1.593
	Numbers of cations (1) (2)									
3)	0.675	0.031	0.251	0.182	0.004	0.323	0.207	0.071	0.020	
	Total # of oxygens (3)									
4)	1.350	0.061	0.377	0.182	0.004	0.323	0.207	0.035	0.010	2.551

5) Oxygen factor (4) (23)/(2.551) = 9.02

Cations per 23 oxygens (5)

	Si	Ti	Al	Fe_{total}	Mn	Mg	Ca	Na	K	sum
6)	6.09	0.28	2.27	1.65	0.03	2.91	1.87	0.64	0.18	15.91

fO_2 and Fe^{3+} and Fe^{2+} in amphibole

	$\log[fO_2]$ (6)	Fe^{3+}/Fe^{2+} (7)	Fe^{3+} (8)	Fe^{2+} (8)
7)	-11.42	0.10	0.14	1.50

T cations (9)

	Si	Al(IV)	Ti	sum T
	6.09	1.91	0.00	8.00

C cations (9)

	Al(VI)	Cr	Fe^{3+}	Ti	Mg	Fe	sum C
8)	0.36	0.00	0.14	0.28	2.91	1.31	5.00

B Cations (9)

	Fm	Ca	Na	sum B
9)	0.22	1.78	0.00	2.00

Classification (9)

$(Ca+Na)_B$	Na_B	Group
1.78 (≥1.0)	0.0 (≤0.5)	CALCIC

(1) Mole proportions in row 2 are weight % values divided by the molecular weight of the oxides as indicated. Numbers of cations (row 3) are obtained by multiplying mole proportions (row 2) by the numbers of cations per oxide, i.e., Al_2O_3 has two cations per formula unit, and so its mole proportion, 0.126, is multiplied by 2. (2) All calculations are carried out without rounding; the value 0.251 for Al_2O_3 is the rounded value for the product of 2 x the un-rounded mole proportion of Al_2O_3. (3) Total number of oxygens (row 4) represents mole proportions (row 2) multiplied by the numbers of oxygens for each oxide; so Al_2O_3, having 3 oxygens, its mole proportion is multiplied by 3. (4) The oxygen factor (row 5) is the number of oxygens (23) for a given mineral formula, here taken as 23 for amphibole (or more strictly, a -46 charge, derived from 23 O^{2-}, or $22O^{2-} + 2(OH)^-$ per formula unit), divided by the sum of row 4), total oxygens. (5) Cations on a 23 oxygen basis (row 6) are derived by multiplying numbers of cations (row 3) by the oxygen factor (row 5). The cation sum for amphiboles on a 23 oxygen basis should be between 15 and 16. (6) Log[fO_2] is calculated from Putirka (2016; in review) assuming QFM and $T = 952^oC$. (7) Ferric-ferrous ratios in amphibole are assumed to be identical to those in an equilibrated liquid (King et al. 2000). (8) Fe^{3+} in amphibole = $(Fe_{total})(r)/(1 + 2r)$, where Fe_{total} are total Fe cations on a 23 oxygen basis (row 6), and $r = Fe^{3+}/Fe^{2+}$; $Fe^{2+} = Fe_{total} - Fe^{3+}$. (9) T = tetrahedral cations; T, B and C cations (rows 7-9), and classification scheme are calculated as in Leake et al. (1997).

Table 4c. Example of Liquid Component and P-T Calculations

Inferred Liquid Composition

Weight % (1)

	SiO_2	TiO_2	Al_2O_3	FeOt	MnO	MgO	CaO	Na_2O	K_2O	P_2O_5	H_2O	Sum
1)	62.317	0.593	17.015	5.579	0.147	1.494	5.199	3.800	3.840	0.321	5.000	
Mole proportions												
2)	1.037	0.007	0.167	0.078	0.002	0.037	0.093	0.061	0.041	0.002	0.278	1.80
Hydrous Mole fractions												
3)	0.575	0.004	0.093	0.043	0.001	0.021	0.051	0.034	0.023	0.001	0.154	1.00

4) $K_D(Fe\text{-}Mg)^{amph\text{-}liq}$ 0.27 **(2)** $Fe\#^{amph}$ = 0.361 SiO_2 = 58.3 wt. %

***P*(kbar)** ***T*(°C)**

	Eqn. 7a	Eqn. 7b	Eqn. 7c	Eqn. 5	Eqn. 6	Si in Hbl	Eqn. 3	Eqn. 4a	Eqn. 4b	Eqn. 8	Eqn. 9
5)	6.2	4.3	6.7	956	952	975	942	956	927	947	963

***P*(kbar) (3)** ***T*(°C) (3)**

	R&R 1a	R&R 1b	R&R 1c	R&R 1d	R&R 1e	R2010	M15; D(Mg)	M15; Liq
6)	5.9	4.2	4.7	5.9	8.1	3.2	910	934

***P*(kbar) (3)**

	H&Z86	H&Z86	H&Z86	H87	J&R89	A&S95	B90	S92
7)	7.5	6.6	7.5	8.0	6.1	-0.8	7.9	7.8

(1) The liquid composition is obtained from mass balance, by mixing mafic and felsic Merapi whole rock compositions, selecting a mixture such that Fe-Mg exchange, between amphibole (amph) and liquid (liq) is equal to 0.27 (Eqn. 2; row 4 in this table). (2) The Fe-Mg exchange coefficient is calculated using the liquid hydrous mole fractions of FeO and MgO (row 3), and the molar ratio of FeO and MgO from Table 4b (row 2); SiO_2 is calculated using Eqn. 10, and is nearly within error of the value obtained using Fe-Mg exchange (62.3%; row 1). (3) R&R = Ridolfi and Renzulli (2011); M15 = Molina et al. (2015); H&Z86 = Hammerstrom and Zen (1986); H87 = Hollister et al. (1987); J&R89 = Johnson and Rutherford (1989); A&S95 = Anderson and Smith (1995); B90 = Blundy and Holland (1990); S92 = Schmidt (1992).

Figure 1

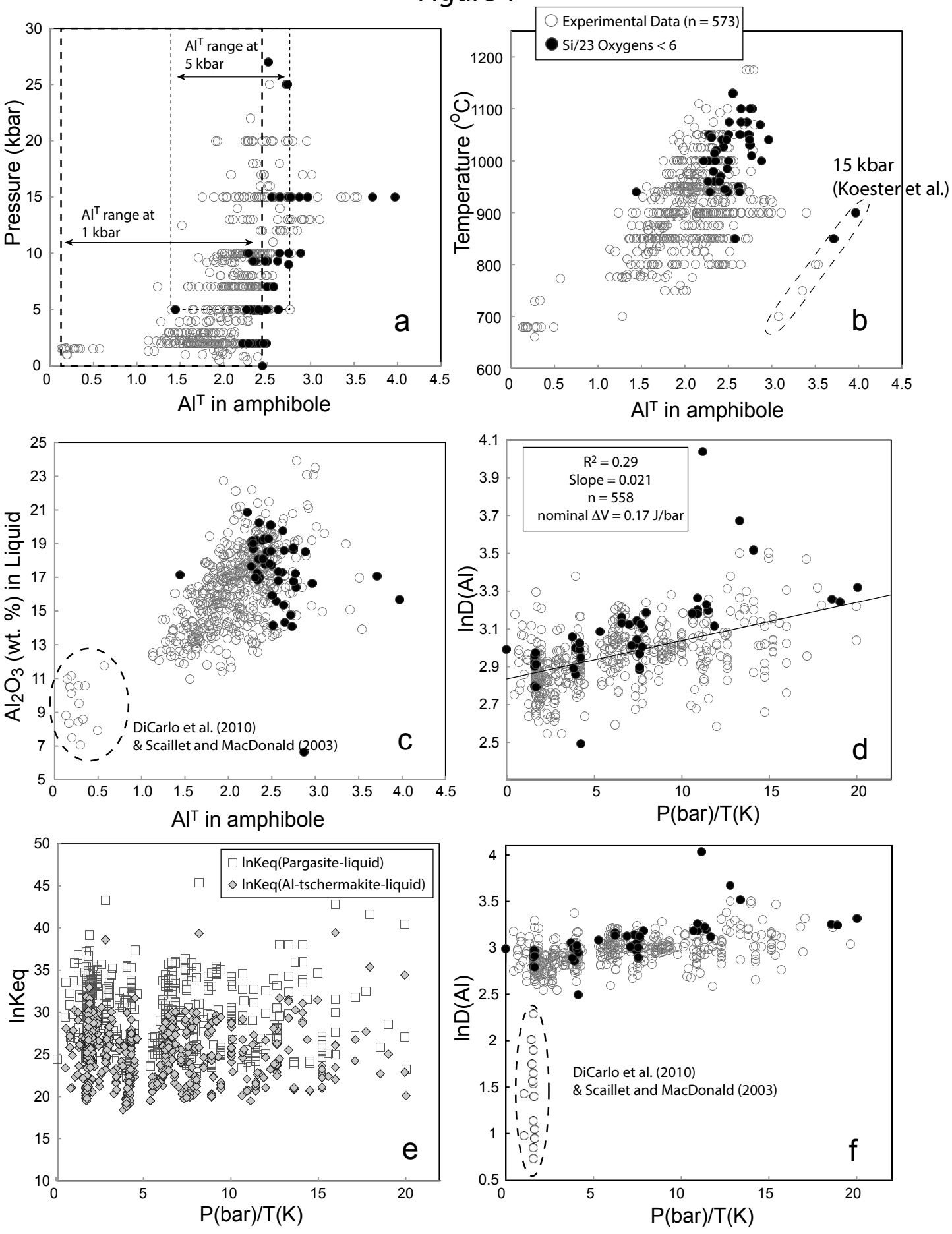
Pressure (kbar)
Al^T in amphibole
Al^T range at 5 kbar
Al^T range at 1 kbar
a
Experimental Data (n = 573)
Si/23 Oxygens < 6
Temperature (°C)
15 kbar (Koester et al.)
b
Al2O3 (wt. %) in Liquid
DiCarlo et al. (2010) & Scaillet and MacDonald (2003)
c
R² = 0.29
Slope = 0.021
n = 558
nominal ΔV = 0.17 J/bar
lnD(Al)
P(bar)/T(K)
d
lnKeq(Pargasite-liquid)
lnKeq(Al-tschermakite-liquid)
lnKeq
e
f

Figure 2

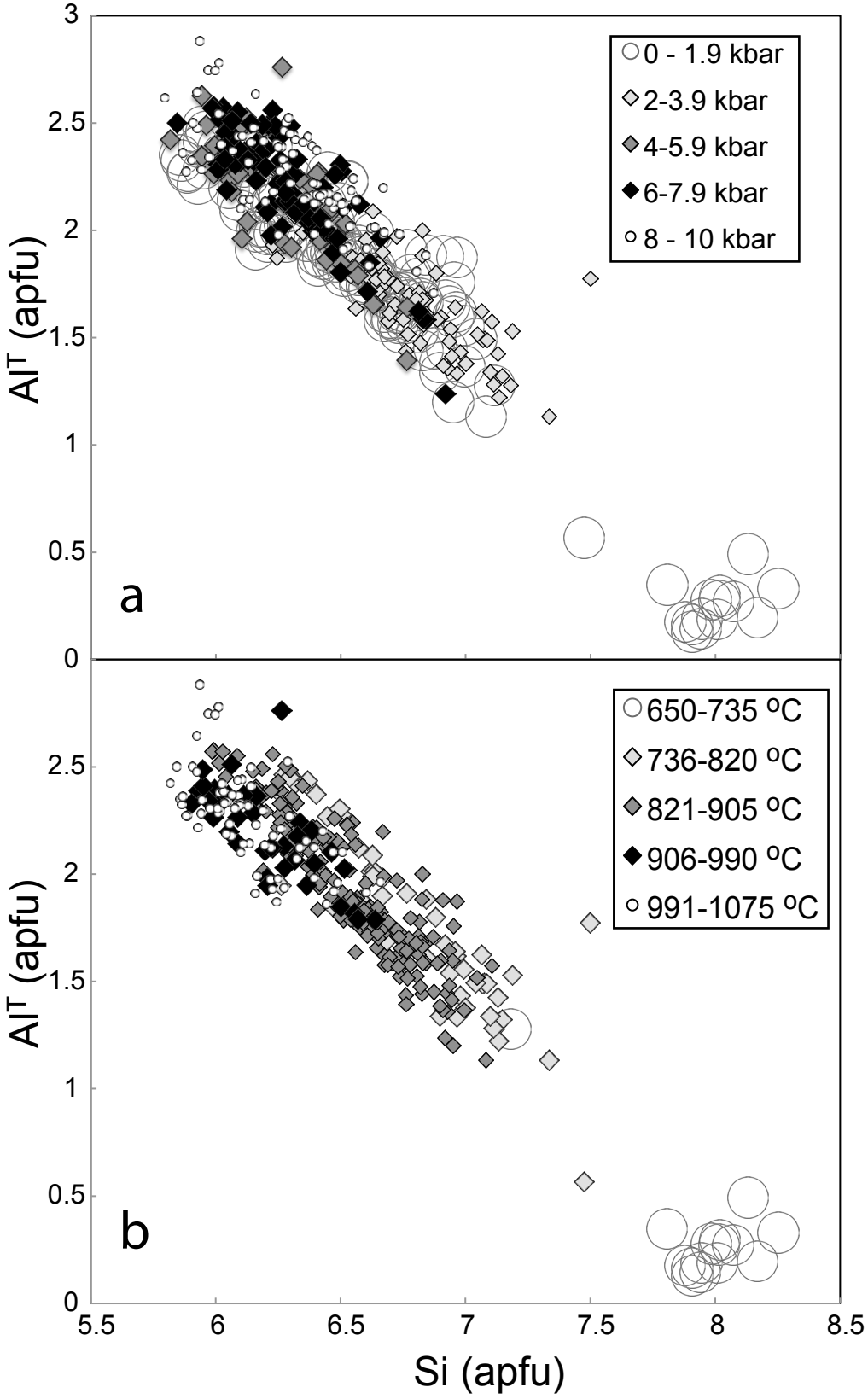
0 - 1.9 kbar
2-3.9 kbar
4-5.9 kbar
6-7.9 kbar
8 - 10 kbar
650-735 ºC
736-820 ºC
821-905 ºC
906-990 ºC
991-1075 ºC
AlT (apfu)
Si (apfu)
a
b
0
0.5
1
1.5
2
2.5
3
5.5
6
6.5
7
7.5
8
8.5

This is a preprint, the final version is subject to change, of the American Mineralogist (MSA)
Cite as Authors (Year) Title. American Mineralogist, in press.
(DOI will not work until issue is live.) DOI: http://dx.doi.org/10.2138/am-2016-5506

Figure 3

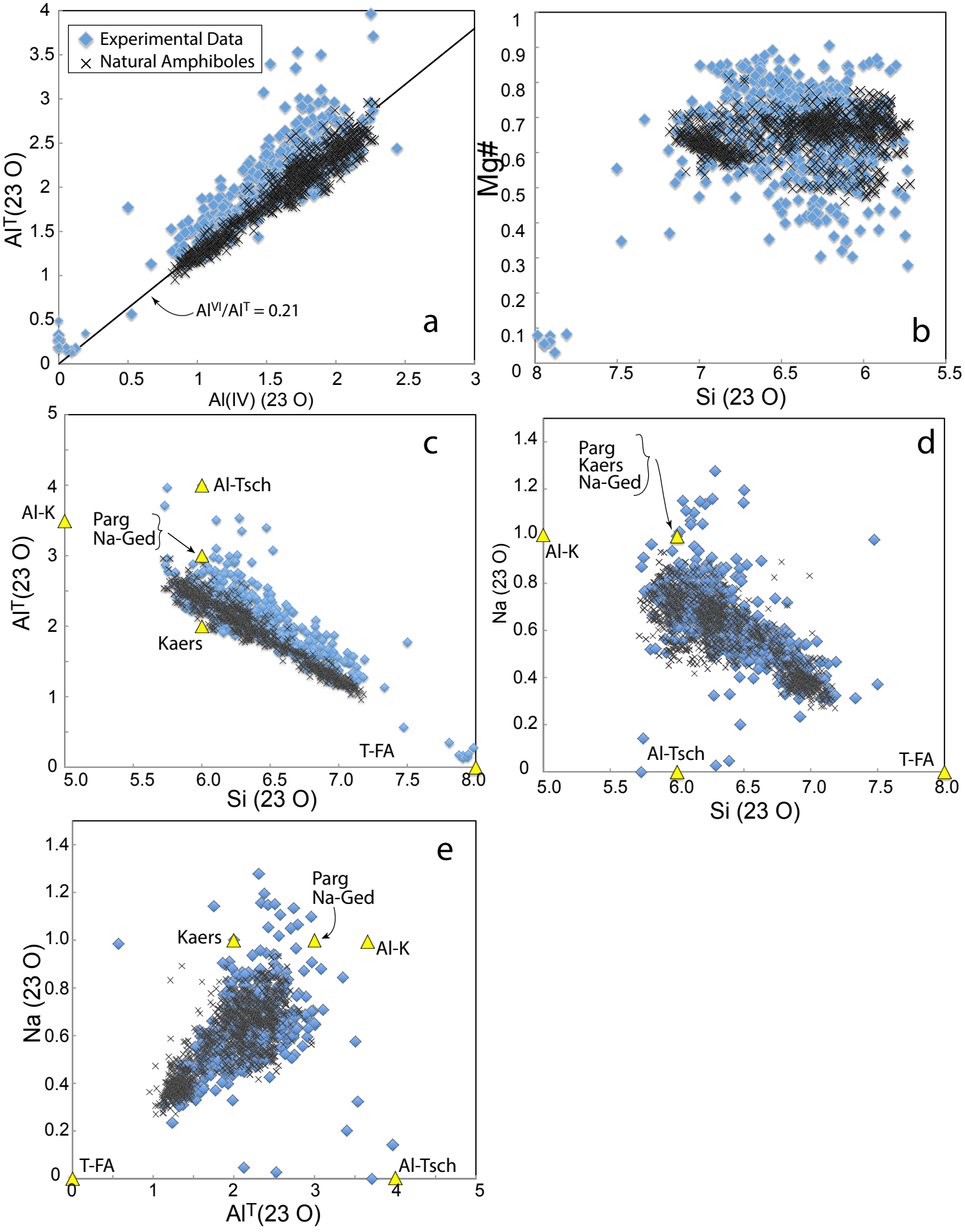

Figure 4

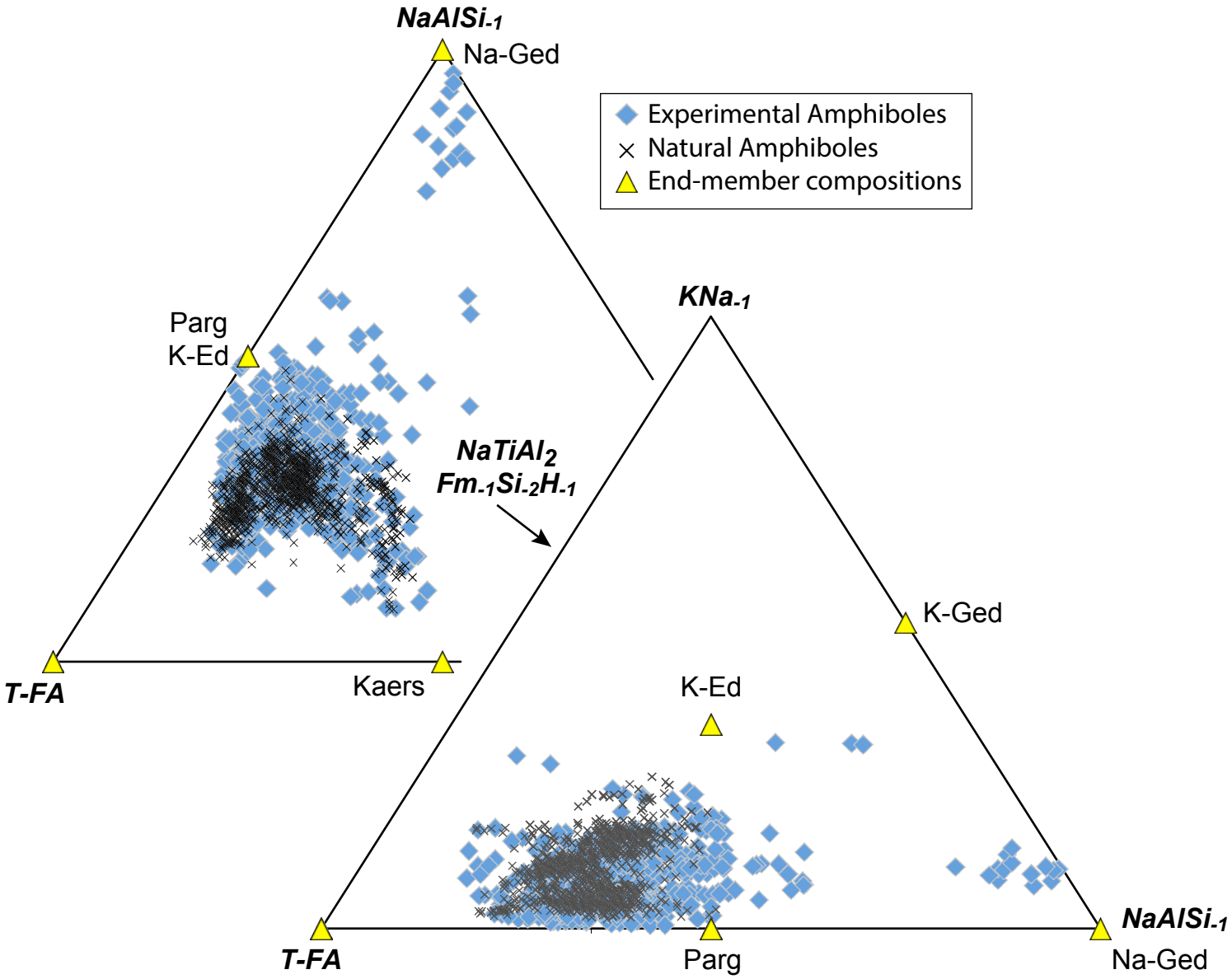
NaAlSi-1
Na-Ged
Experimental Amphiboles
Natural Amphiboles
End-member compositions
Parg
K-Ed
NaTiAl2
Fm-1Si-2H-1
T-FA
Kaers
KNa-1
K-Ged
K-Ed
T-FA
Parg
NaAlSi-1
Na-Ged

Figure 5a-d

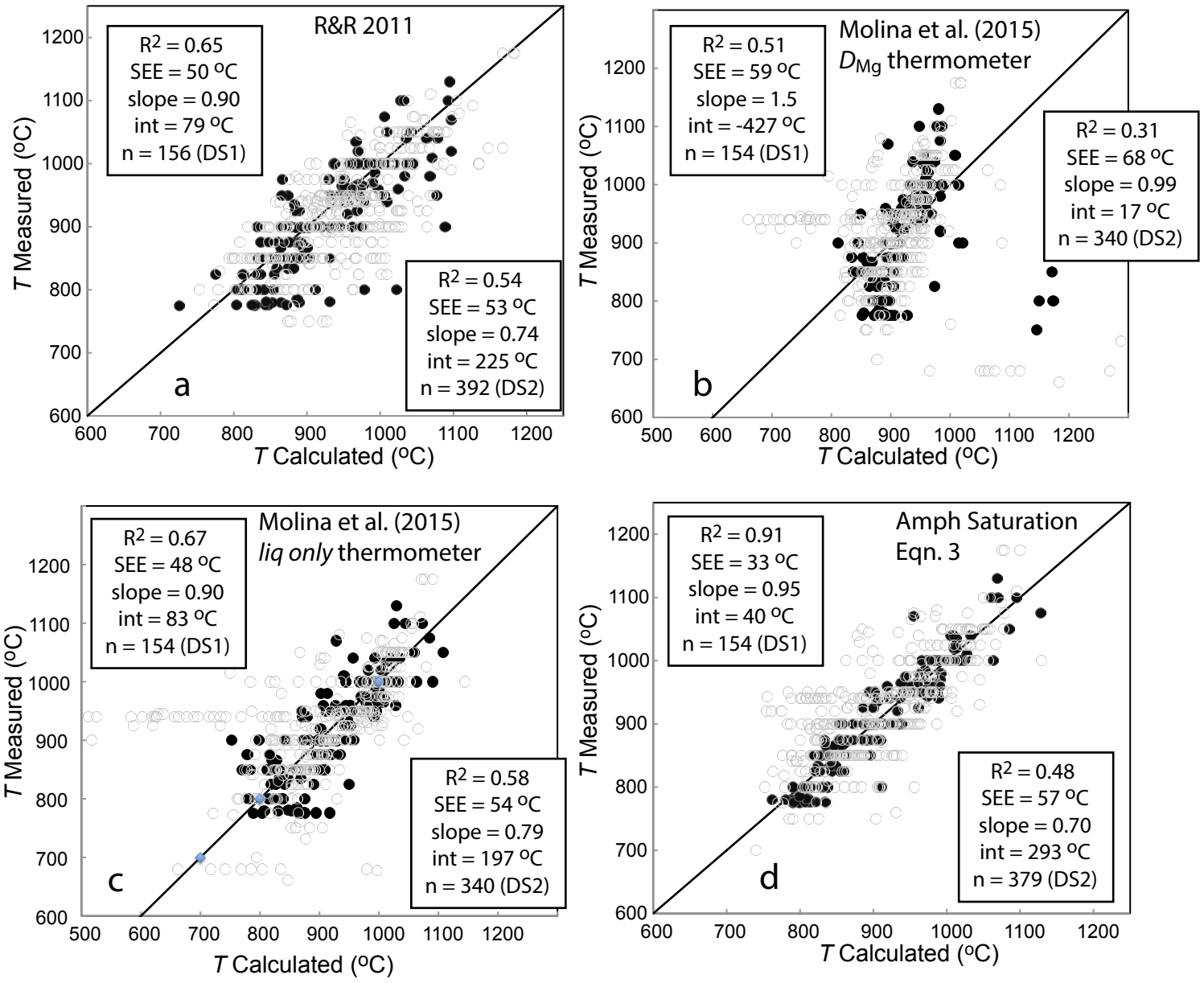
R&R 2011
R2 = 0.65
SEE = 50 °C
slope = 0.90
int = 79 °C
n = 156 (DS1)
R2 = 0.54
SEE = 53 °C
slope = 0.74
int = 225 °C
n = 392 (DS2)
a
Molina et al. (2015)
DMg thermometer
R2 = 0.51
SEE = 59 °C
slope = 1.5
int = -427 °C
n = 154 (DS1)
R2 = 0.31
SEE = 68 °C
slope = 0.99
int = 17 °C
n = 340 (DS2)
b
Molina et al. (2015)
liq only thermometer
R2 = 0.67
SEE = 48 °C
slope = 0.90
int = 83 °C
n = 154 (DS1)
R2 = 0.58
SEE = 54 °C
slope = 0.79
int = 197 °C
n = 340 (DS2)
c
Amph Saturation
Eqn. 3
R2 = 0.91
SEE = 33 °C
slope = 0.95
int = 40 °C
n = 154 (DS1)
R2 = 0.48
SEE = 57 °C
slope = 0.70
int = 293 °C
n = 379 (DS2)
d
T Measured (°C)
T Calculated (°C)

Figure 5e-h

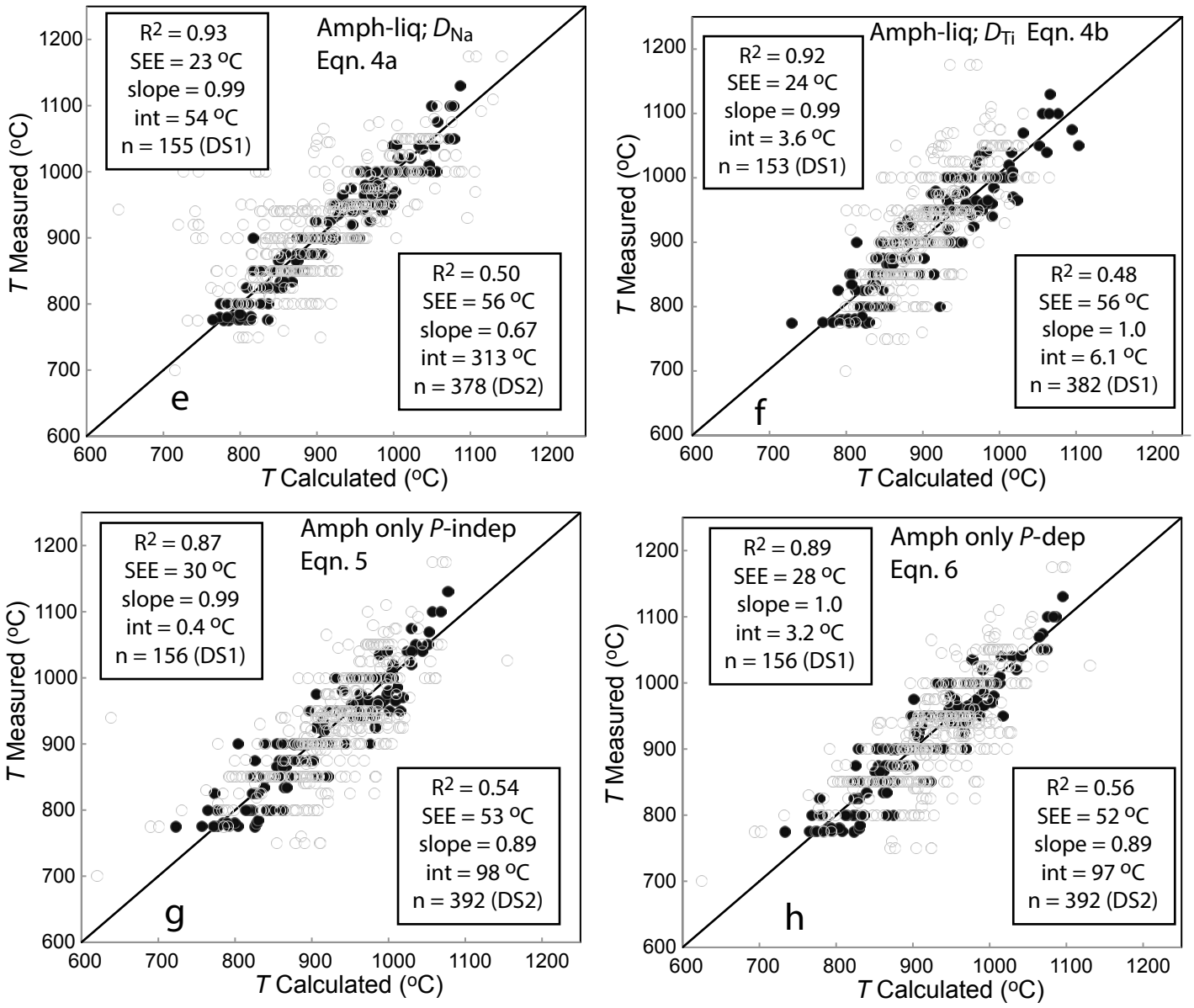
R2 = 0.93
SEE = 23 oC
slope = 0.99
int = 54 oC
n = 155 (DS1)
Amph-liq; DNa
Eqn. 4a
R2 = 0.50
SEE = 56 oC
slope = 0.67
int = 313 oC
n = 378 (DS2)
e
T Measured (oC)
T Calculated (oC)
R2 = 0.92
SEE = 24 oC
slope = 0.99
int = 3.6 oC
n = 153 (DS1)
Amph-liq; DTi Eqn. 4b
R2 = 0.48
SEE = 56 oC
slope = 1.0
int = 6.1 oC
n = 382 (DS1)
f
R2 = 0.87
SEE = 30 oC
slope = 0.99
int = 0.4 oC
n = 156 (DS1)
Amph only P-indep
Eqn. 5
R2 = 0.54
SEE = 53 oC
slope = 0.89
int = 98 oC
n = 392 (DS2)
g
R2 = 0.89
SEE = 28 oC
slope = 1.0
int = 3.2 oC
n = 156 (DS1)
Amph only P-dep
Eqn. 6
R2 = 0.56
SEE = 52 oC
slope = 0.89
int = 97 oC
n = 392 (DS2)
h

This is a preprint, the final version is subject to change, of the American Mineralogist (MSA)
Cite as Authors (Year) Title. American Mineralogist, in press.
(DOI will not work until issue is live.) DOI: http://dx.doi.org/10.2138/am-2016-5506

Figure 6a-f

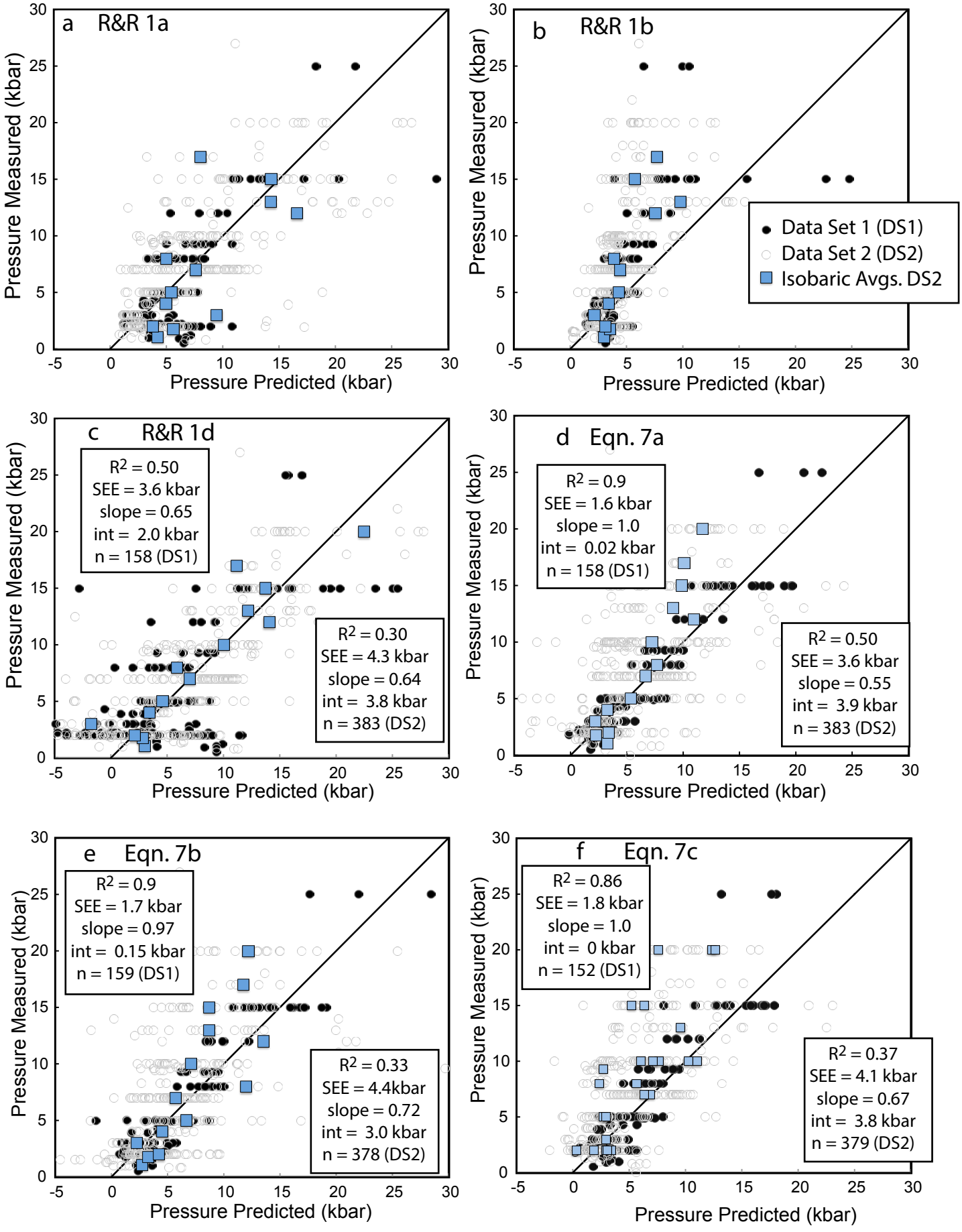

Figure 6g-j

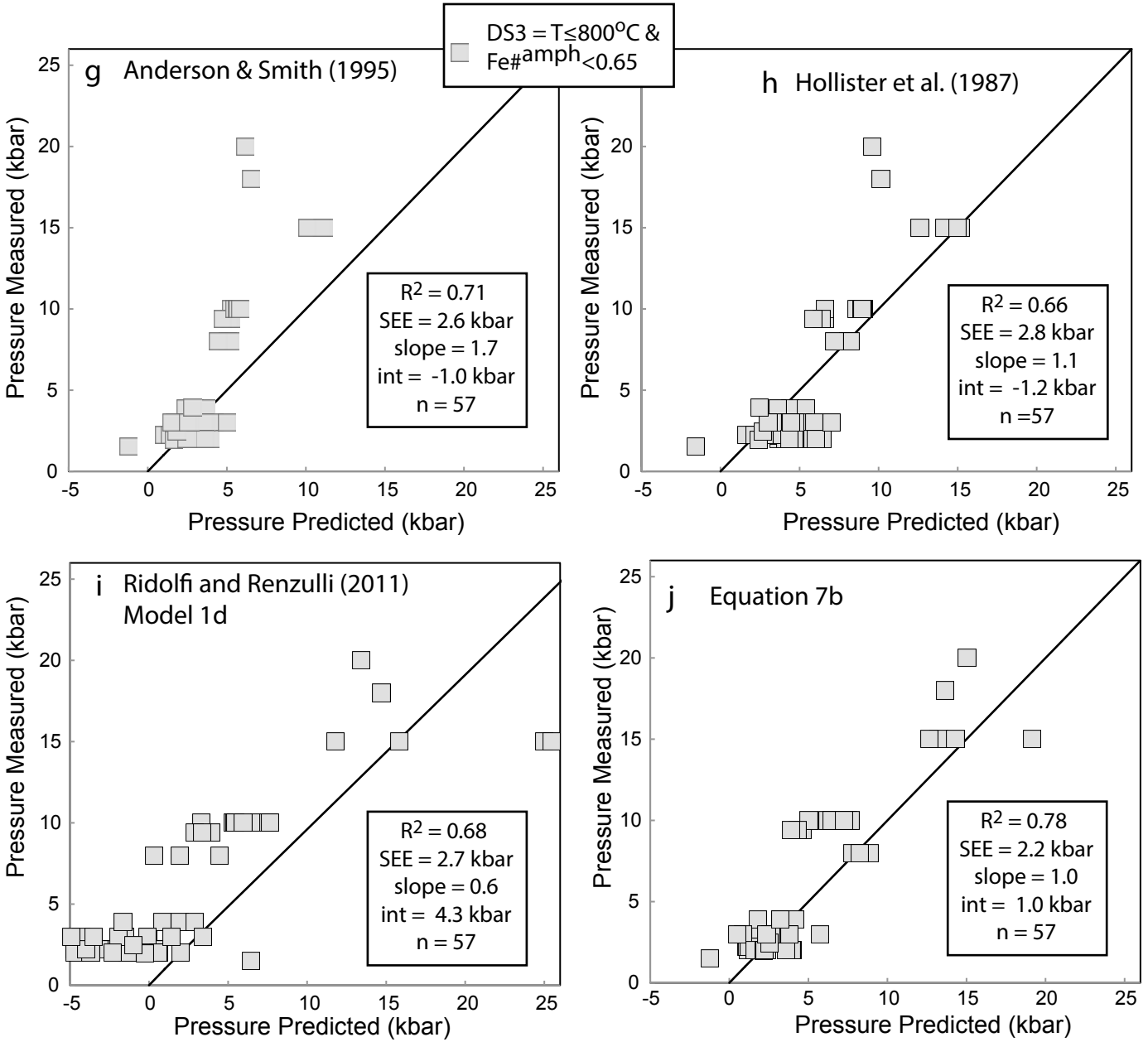
DS3 = T≤800°C & Fe#amph<0.65
g Anderson & Smith (1995)
h Hollister et al. (1987)
i Ridolfi and Renzulli (2011) Model 1d
j Equation 7b
Pressure Measured (kbar)
Pressure Predicted (kbar)
R2 = 0.71
SEE = 2.6 kbar
slope = 1.7
int = -1.0 kbar
n = 57
R2 = 0.66
SEE = 2.8 kbar
slope = 1.1
int = -1.2 kbar
n =57
R2 = 0.68
SEE = 2.7 kbar
slope = 0.6
int = 4.3 kbar
n = 57
R2 = 0.78
SEE = 2.2 kbar
slope = 1.0
int = 1.0 kbar
n = 57

Figure 7

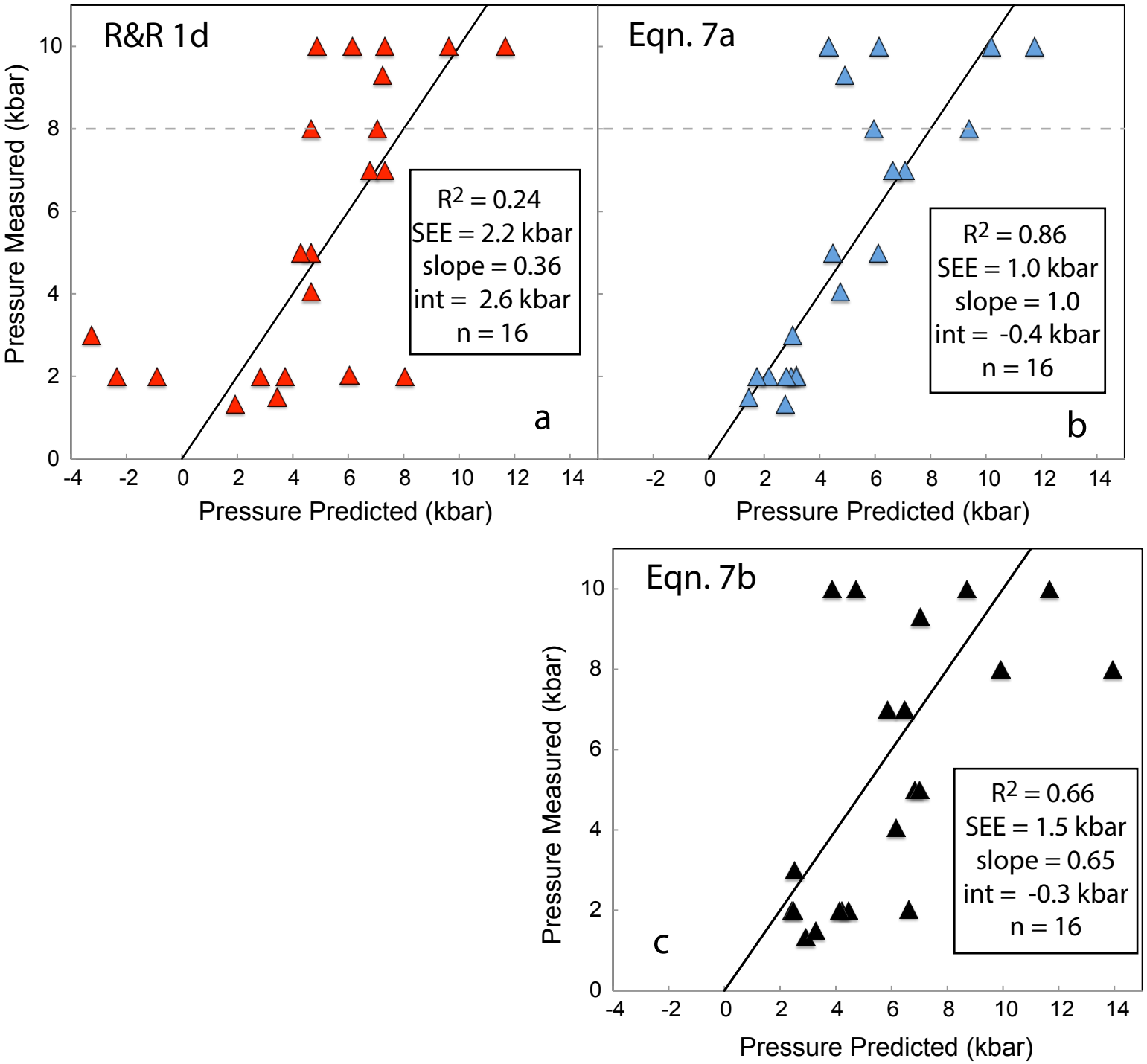
R&R 1d
Pressure Measured (kbar)
Pressure Predicted (kbar)
R2 = 0.24
SEE = 2.2 kbar
slope = 0.36
int = 2.6 kbar
n = 16
a
Eqn. 7a
R2 = 0.86
SEE = 1.0 kbar
slope = 1.0
int = -0.4 kbar
n = 16
b
Eqn. 7b
R2 = 0.66
SEE = 1.5 kbar
slope = 0.65
int = -0.3 kbar
n = 16
c

Figure 8

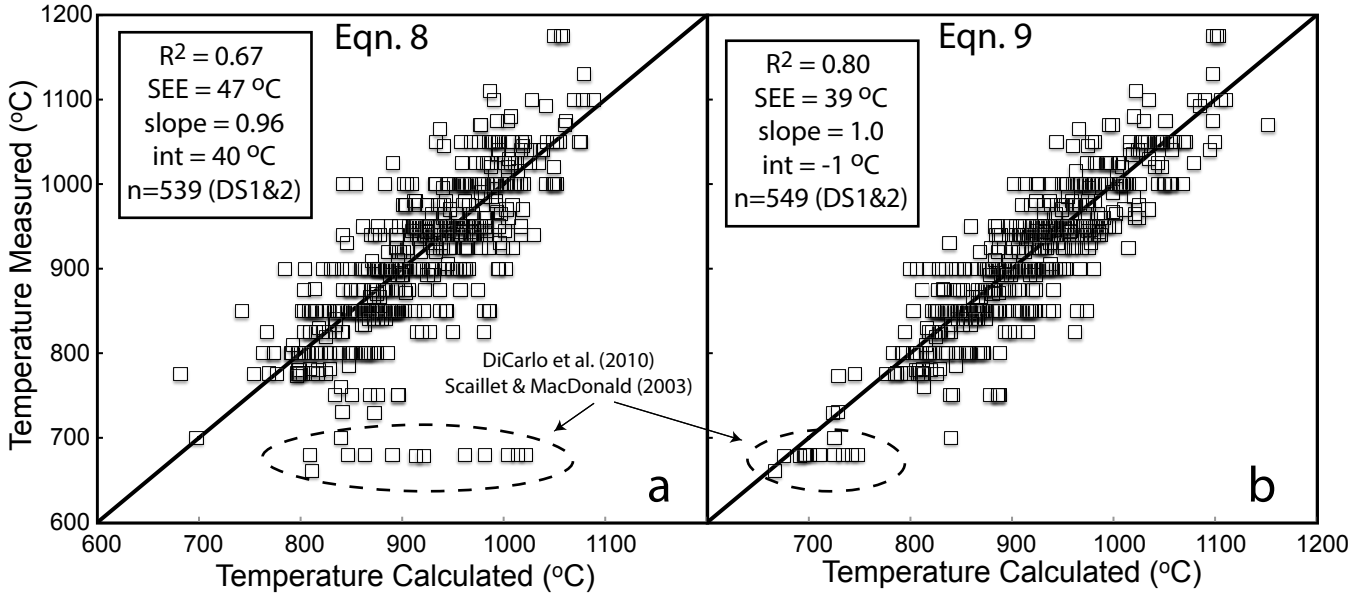
Eqn. 8
R2 = 0.67
SEE = 47 °C
slope = 0.96
int = 40 °C
n=539 (DS1&2)
DiCarlo et al. (2010)
Scaillet & MacDonald (2003)
a
Eqn. 9
R2 = 0.80
SEE = 39 °C
slope = 1.0
int = -1 °C
n=549 (DS1&2)
b
Temperature Measured (°C)
Temperature Calculated (°C)
Temperature Calculated (°C)
600
700
800
900
1000
1100
1200

Figure 9

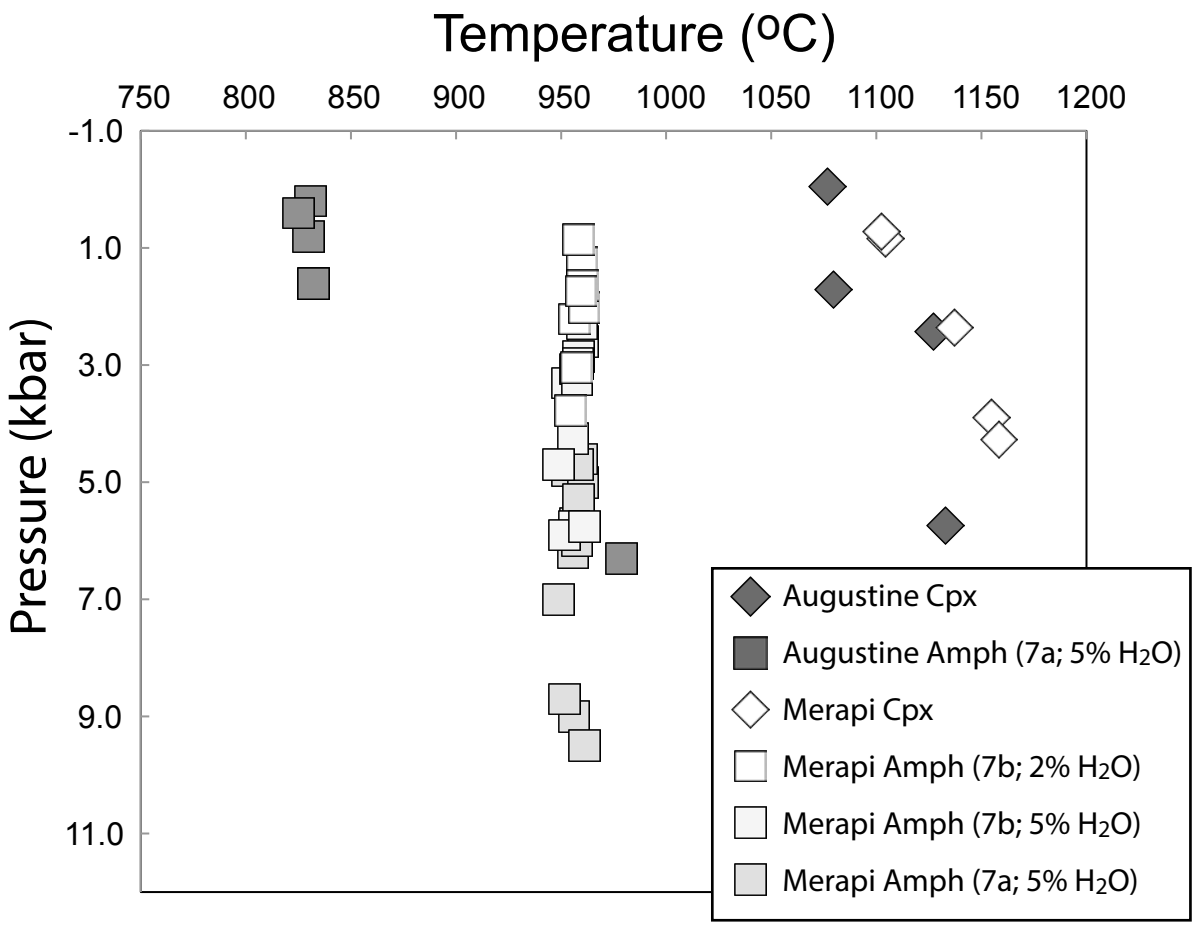
Temperature (ºC)
750
800
850
900
950
1000
1050
1100
1150
1200
Pressure (kbar)
-1.0
1.0
3.0
5.0
7.0
9.0
11.0
Augustine Cpx
Augustine Amph (7a; 5% H2O)
Merapi Cpx
Merapi Amph (7b; 2% H2O)
Merapi Amph (7b; 5% H2O)
Merapi Amph (7a; 5% H2O)